

**UCSF**

**UC San Francisco Electronic Theses and Dissertations**

**Title**

Probing the consequences of cell-to-cell variability during epithelial morphogenesis: a programmed assembly approach

**Permalink**

<https://escholarship.org/uc/item/6d47c2q2>

**Author**

Liu, Jennifer S.E.

**Publication Date**

2013

Peer reviewed|Thesis/dissertation

Probing the consequences of cell-to-cell variability  
during epithelial morphogenesis: a programmed assembly approach

by

Jennifer S.E. Liu

DISSERTATION

Submitted in partial satisfaction of the requirements for the degree of

DOCTOR OF PHILOSOPHY

in

Chemistry and Chemical Biology

in the

GRADUATE DIVISION

of the

UNIVERSITY OF CALIFORNIA, SAN FRANCISCO

Copyright (2013)

By

Jennifer S.E. Liu

## Acknowledgements

First and foremost, I would like to thank my family. They keep me grounded when life feels overwhelming, and always support and believe in me. I also need to acknowledge my friends, especially Sindy and Andy, who have stuck by me through good times and bad. I hope we are older and wiser for the adventures we've shared together.

My graduate experience in the Gartner lab has felt like a real journey, starting with the logistical details of establishing a lab space and recruiting other lab members, and ending with a validated technology and conceptual framework for studying the consequences of tissue heterogeneity. The work in this dissertation would not have been possible without the guidance of Professor Zev Gartner. His constant support and enthusiasm helped turn an unexpected observation into a project with real implications in cell, tissue, and cancer biology. I also thank the other Gartner lab members for sharing their friendship and intellect.

I would like to thank Professors Mark LaBarge, Mina Bissell, Jay Debnath, and Keith Mostov for providing the advice and expertise we needed to apply a chemical biology technology to biologically-relevant and interesting model systems. Professors Jack Taunton, Kevan Shokat, and Pam England were kind enough to share facilities and reagents, and the UCSF Viracore and Laboratory for Cell Analysis were instrumental for a number of the enclosed studies.

Part of this dissertation is a reproduction of material previously published and contains contributions from collaborators listed therein. Chapter 1 is



reproduced in part with permission from Liu, J.S.; Gartner, Z.J., 2012. Directing the assembly of spatially organized multicomponent tissues from the bottom up. *Trends in Cell Bio* 22, 683-691. Chapters 2, 3, and 4 are reproduced in part with permission from Liu, J.S.; Farlow, J.T.; Paulson, A.; LaBarge, M.A.; Gartner, Z.J., 2012. Programmed Cell-to-Cell Variability in Ras Activity Triggers Emergent Behaviors during Mammary Epithelial Morphogenesis. *Cell Reports* 2, 1461-1470.

## Abstract

The formation, maintenance, and function of epithelial tissues are guided by dynamic interaction between epithelial cells and their surrounding microenvironment. Three-dimensional (3D) epithelial cell culture models are valuable *ex vivo* tools for understanding the global effects of soluble factors, extracellular matrix components, and genetic perturbations on multicellular processes such as morphogenesis and tissue polarization. Probing the consequences of cell-to-cell variability in the activation of specific pathways remains challenging even in 3D culture models, however, because controlling the patterns of variability within each multicellular structure has been difficult under the culture conditions necessary to support morphogenesis.

To better model cell-to-cell variability within heterogeneous epithelia, we are using a DNA-templated programmed assembly strategy to build aggregates of MCF10A human mammary epithelial cells with defined cell number, composition, and initial cell-cell connectivity. We do so by labeling cell surfaces with synthetic, single-stranded DNA and directing the assembly of complementarily labeled cell populations. When grown in 3D culture, assembled wild-type (WT) aggregates condense into polarized microtissues that undergo morphogenesis. MCF10A aggregates expressing low levels of oncogenic H-Ras (MCF10A<sup>Ras</sup>) similarly polarize and undergo morphogenesis. Surprisingly, heterogeneous aggregates where single MCF10A<sup>Ras</sup> cell are assembled with WT cells display emergent phenotypes such as cell extrusions and multicellular protrusions. These results add to accumulating evidence that emergent

behaviors may arise from heterogeneity within local populations of epithelial cells and highlight the utility of our bottom-up method for constructing mosaic epithelial microtissues for studying such interactions in defined microenvironments. Understanding the mechanisms and conditions required for such emergent behaviors may inform upon similar behaviors observed in early stages of cancer development and progression.

# TABLE OF CONTENTS

<b>CHAPTER 1 INTRODUCTION</b>	<b>1</b>
<i>Investigating the relationship between tissue form and function with in vitro engineered tissues</i>	2
<i>Bottom-up, programmed assembly approaches</i>	5
<i>Three-dimensional cell culture</i>	12
<i>References</i>	15
<b>CHAPTER 2 PROGRAMMED ASSEMBLY OF EPITHELIAL MICROTISSUES</b>	<b>23</b>
<i>Introduction</i>	24
<i>Results</i>	28
DNA-templated programmed assembly	28
3D culture of homogeneous MCF10A assemblies	32
<i>Discussion</i>	37
<i>Methods</i>	39
<i>References</i>	45
<b>CHAPTER 3 CONSEQUENCES OF CELL-TO-CELL VARIABILITY IN EPITHELIAL MICROTISSUES</b>	<b>49</b>
<i>Introduction</i>	50
<i>Results</i>	53

Emergent behaviors in assemblies with controlled cell-to-cell variability in Ras pathway activation	53
Suppression of proliferation mutants within MCF10A acini	61
Towards building bilayered structures using programmed assembly	63
<i>Discussion</i>	65
<i>Methods</i>	69
<i>References</i>	72
<b>CHAPTER 4 MOLECULAR CHARACTERIZATION OF RAS-DRIVEN EMERGENT BEHAVIORS</b>	<b>79</b>
<i>Introduction</i>	80
<i>Results</i>	81
Inhibition of effectors downstream of Ras	81
Investigating the role of paracrine signaling molecules	85
Heterogeneity in E-cadherin expression in MCF10A <sup>Ras</sup> cell line	89
<i>Discussion</i>	92
<i>Methods</i>	94
<i>References</i>	97
<b>CONCLUSION AND PERSPECTIVE</b>	<b>101</b>
<b>APPENDIX 1 CHEMICAL SCHEMES</b>	<b>105</b>
<b>APPENDIX 2 SUPPLEMENTAL FIGURES AND TEXT</b>	<b>107</b>

<i>Supplemental Figures</i>	108
<i>Supplemental Text</i>	111
<b>APPENDIX 3 LIST OF PUBLICATIONS</b>	<b>113</b>

## TABLE OF FIGURES

<b>FIGURE 1-1.</b> Cross section illustrating tissue architecture changes in healthy and cancerous mammary gland ducts.	4
<b>FIGURE 1-2.</b> Examples of modular repeating units found in mammalian tissues.	7
<b>FIGURE 1-3.</b> DNA-templated programmed assembly method.	11
<b>FIGURE 2-1.</b> The modular and hierarchical organization of the human mammary gland.	25
<b>FIGURE 2-2.</b> Different techniques for labeling cell surfaces with ssDNA.	27
<b>FIGURE 2-3.</b> ssDNA labeling in model breast epithelial cell lines.	30
<b>FIGURE 2-4.</b> Programmed assembly of homogeneous and heterogeneous structures.	32
<b>FIGURE 2-5.</b> Transfer of assembled aggregates into 3D culture.	34
<b>FIGURE 2-6.</b> Onset of polarity, growth arrest, and lumen formation in MCF10A cell aggregates.	37
<b>FIGURE 3-1.</b> Assembled MCF10ARas cells undergo morphogenesis similar to MCF10A WT cells.	55
<b>FIGURE 3-2.</b> Emergent behaviors in microtissues heterogeneous for signaling downstream of H-Ras.	57
<b>FIGURE 3-3.</b> Characterization of emergent behaviors by microscopy.	58

<b>FIGURE 3-4.</b> Quantitative analysis of cell motility during emergent behaviors.	61
<b>FIGURE 3-5.</b> Cell suppression in developing acini.	63
<b>FIGURE 3-6.</b> 3D culture of heterogeneous assemblies containing NME-1 cells.	65
<b>FIGURE 4-1.</b> Treatment of emergent phenotypes with small-molecule inhibitors of Ras effectors.	83
<b>FIGURE 4-2.</b> RNAi of MEK1 in specific assembly population.	84
<b>FIGURE 4-3.</b> Effects of media condition manipulation on phenotype distribution.	87
<b>FIGURE 4-4.</b> Effects of secreted signaling molecules on phenotype distribution.	89
<b>FIGURE 4-5.</b> Extrusion phenotype associated with low E-cadherin expression of MCF10ARas cells.	91
<b>FIGURE 4-6.</b> Cell intrinsic differences in MCF10A <sup>Ras</sup> clones.	92
<b>SUPPLEMENTAL FIGURE S1.</b> Polarity of homogeneous microtissues.	108
<b>SUPPLEMENTAL FIGURE S2.</b> Characterization of emergent phenotypes.	109
<b>SUPPLEMENTAL FIGURE S3.</b> Tracking data for H2B-GFP-expressing MCF10A <sup>Ras</sup> cells in WT microtissues exhibiting normal, basal extruding, or motile multicellular protrusion phenotypes.	110
<b>SUPPLEMENTAL FIGURE S4.</b> Characterization of MCF10A <sup>ER-Ras</sup> cells.	112



# **CHAPTER 1**

## **INTRODUCTION**

Source: The following chapter was published in part as a review from Liu, J.S. and Gartner, Z.J., 2012. Directing the assembly of spatially organized multicomponent tissues from the bottom up. *Trends in Cell Bio* 22, 683-691.

Contributions: The manuscript is an original review of the literature on bottom-up approaches to building tissue models with multiple cell types. Zev Gartner and I wrote the manuscript, and I wrote the additional text in the Introduction and Three-dimensional culture sections.

## INVESTIGATING THE RELATIONSHIP BETWEEN TISSUE FORM AND FUNCTION WITH *IN VITRO* ENGINEERED TISSUES

Each human being contains trillions of cells spanning over 200 specialized subtypes. This complex cellular community grows within a web of extracellular matrix (ECM) to form the tissues and organs that perform the numerous functions of our bodies. Cells, tissues, and organs constitute a hierarchy of structures spanning tens of microns to meters, in which the arrangement of building blocks at one scale forms the building block for the next. The proper arrangement of many individual cells, often of different cell types, into a specific structure is therefore required for proper tissue and organ function, and failure to maintain or restore healthy tissue structure is associated with diseases such as cancer.

Within the location imposed by tissue structure, an individual cell's behavior is directly influenced by its microenvironment. The microenvironment is composed of soluble factors, ECM, and other cells. To accurately model and understand physiologically relevant cell behaviors, we would ideally recreate the *in vivo* microenvironment when studying cells in more tractable *ex vivo* settings. Soluble factors and ECM components of the microenvironment can typically be identified and added exogenously into culture conditions. Recapitulating the cellular component of the microenvironment in the correct multicellular architecture, however, can be difficult. *In vivo*-like architectures can sometimes be attained using stem cells with intact developmental programs. In a few special cases, separated cell populations that have been purified from tissues will

spontaneously organize into structures reminiscent of the tissue of origin. Unfortunately, in the majority of cases, it is not possible to design *in vivo*-like cellular microenvironments because direct and general methods for controlling the relative spatial position of cells in models of tissues and organs do not exist.

As 85% of all cancers are of epithelial origin, epithelial tissues such as the mammary gland are microenvironments of special interest to the medical community. In healthy mammary epithelial tissues, individual cells are physically, biochemically, and mechanically coupled to one another. These cell-cell interactions detect and integrate community-level signals, and are required for the proper function of the overall tissue. In pre-cancerous tissues, mutations in individual cells can compromise normal cell-cell communication (Figure 1-1). Though these mutant cells themselves often exhibit aberrant behaviors, the breakdown of interactions between the mutant and surrounding wild-type (WT) cells also needs to be studied to fully understand cancer progression.

One reason that the relationship between heterogeneous cells, such as mutant and WT epithelial cells, in breast cancer has been difficult to study is because the basic tissue architecture is disrupted (Hansen and Bissell, 2000) (Figure 1-1). Such disease-related morphological changes are revealed by histological studies of tissue specimen biopsies. Though histological studies examine diseased ductal architectures in the most relevant *in vivo* settings, they suffer from low throughput, present information from a static moment after disease onset, and do not allow for genetic or structural manipulation of the constituent cells. As a consequence, they cannot be used to understand the

sequence of events that trigger healthy tissue to transition to pre-cancerous and diseased states.

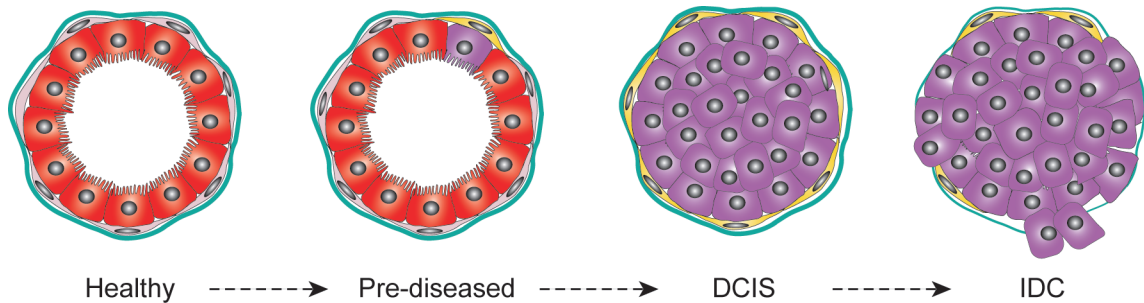


**FIGURE 1-1. Cross section illustrating tissue architecture changes in healthy and cancerous mammary gland ducts.** Healthy mammary gland ducts contain an inner layer of luminal epithelial cells (LEPs, red) surrounded by a layer of myoepithelial cells (MEPs, pink). Mutations or local perturbations can lead to aberrant LEPs (purple) that fill the duct in ductal carcinoma in situ (DCIS) and later invade out of the mammary epithelium in invasive ductal carcinoma (IDC). Mutant LEPs can also lead to cancer-associated MEPs (yellow) that lose tumor suppressor abilities and decrease in number as carcinoma progresses.

A number of challenges face the design of multicellular, epithelial structures with the single-cell resolution necessary to model cancer initiation or other specific cell-cell interactions. For one, an ideal method should allow for incorporation of multiple cell types that are reflective of the complexity of real human tissues without affecting normal cellular functions. Recent research has highlighted the importance of interactions between heterogeneous cell types on tissue behaviors, whether the interactions occur within an epithelium (Eisenhoffer et al., 2012; Hogan et al., 2009; Johnston, 2009; Leung and Brugge, 2012), between the epithelium and surrounding stroma (Engelhardt et al., 2012), or even between cells in different organ systems (DeNardo et al., 2009). Cell incorporation should also be flexible, such that cells of interest (ex. cancer-associated cells) can be exchanged for control cells (ex. healthy cells) for

functional comparison. Finally, the method should also easily interface with culture techniques that allow for manipulation of the soluble and ECM components of the microenvironment.

## BOTTOM-UP, PROGRAMMED ASSEMBLY APPROACHES

One powerful approach that aims to build biological structures *ex vivo* that are reminiscent of those found in the human body is a tissue engineering strategy. Like studies in model organisms, tissue engineering strategies can incorporate genetically modified cellular building blocks. Unlike studies using model organisms, however, tissue engineering strategies are also compatible with the use of primary or immortalized *human* cells, advanced imaging techniques, and techniques that control the non-cellular components of the microenvironment.

Most tissue engineering approaches are “top-down” and require the use of patterned substrates, molds, or ECM scaffolds to assist cells in finding their appropriate positions and differentiation states within a tissue. In principle, a three-dimensional (3D) scaffold of ECM with the precise composition and organization can provide all the necessary structural and microenvironmental cues to direct the organization of individual cells into a functional tissue or organ, as evidenced by recent experiments using decellularized organs (Ott et al., 2008). However, *de novo* construction of scaffolds with the requisite level of detail at all length scales is not currently possible. As a consequence, tissue reconstruction starting from cells or cell aggregates remains challenging because

mixtures of dissociated cells do not typically reconstitute complex tissue structures or functions without pre-organization into the correct 3D geometry. Therefore, additional means of controlling the spatial organization of cells or groups of cells will facilitate tissue engineering.

Bottom-up or synthetic approaches are emerging as a valuable and alternative means to more prevalent top-down approaches for pre-organizing groups of cells into tissue-like structures. Bottom-up approaches are distinct from top-down approaches in that they link together simplified building blocks to generate objects that are structurally organized at larger length scales (Elbert, 2011). Directing the assembly of building blocks from the bottom up may provide enhanced control over the relative spatial arrangement of cells in engineered tissues when used together with currently available top-down approaches. In addition to the advantages of the top-down tissue engineering strategies outlined above, bottom-up methods have several other desirable features. First, they are inherently modular, allowing for the simple replacement of specific cells or nodes in a network of interacting cells, tissues, or organs. This feature makes bottom-up engineering attractive as a versatile method for incorporating multiple cell types into tissues as well as for building different tissue types or states (e.g. functional or pathological) by interchanging building blocks. Further, these methods are inherently scalable; a large number of nearly identical tissue constructs can be prepared without the need for complex or specialized scaffolds. Finally, bottom-up approaches are ideally suited for studying the direct interactions between individual building blocks. While spatially organizing multiple heterogeneous

cellular interactions can be challenging using top-down tissue engineering approaches, a multiplicity of interacting partners can be systematically incorporated using a modular, bottom-up approach.

Bottom-up approaches can be further refined by using building blocks that are designed to assemble with one another in a specific manner. These directed assembly techniques retain the advantages of bottom-up approaches with the benefit of additional control over the organization of the final structure. With appropriately designed building blocks, directed assembly can be used to organize simple components into larger, more complex structures that mimic the cellular heterogeneity and physical arrangement of modular repeating units found in mammalian tissues (Figure 1-2). In this way, cell-cell interactions can also be programmed into the constructs, though the resolution of these interactions depends on the size of the initial modules.

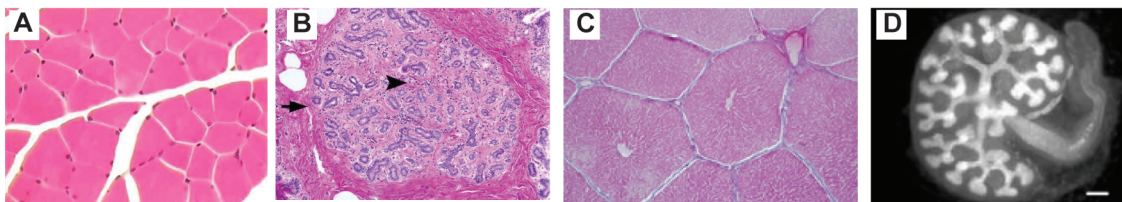


**FIGURE 1-2. Examples of modular repeating units found in mammalian tissues.** (A) Human skeletal muscle cross section (Gustafson, A.W., 1996; <http://ocw.tufts.edu/Content/15/imagegallery/342521/342522/342544>) (B) Human mammary terminal ductal lobular unit cross section (Pathpedia; <http://www.pathpedia.com/education/eatlas/histology/breast/Images.aspx?11>) (C) Pig liver cross section (Werning, S., 2007; [http://calphotos.berkeley.edu/cgi/img\\_query?seq\\_num=223971&one=T](http://calphotos.berkeley.edu/cgi/img_query?seq_num=223971&one=T)) (D) Mouse embryonic kidney (used with permission from Davis, J.A., 2012)

Directed assembly approaches can be used to build spatially defined multicellular structures across a range of tissue-relevant sizes. The minimal

functional unit of many tissues consists of small groups of structurally organized cells embedded in specialized ECM. These structures can be modeled with building blocks of spatially segregated hydrogel units loaded with cells. The explicit inclusion of ECM-like materials is important particularly when matrix components are critical to cell and tissue function, when multiple levels or types of ECM define the functional unit, or when the cells cannot generate the volume and composition of ECM found in biological tissues on their own. Fortunately, many natural and synthetic polymers are available for designing ECM-like hydrogels with specific structural and mechanical properties to mimic different tissues within the human body (Correia and Bissell, 2012; Seliktar, 2012). Due to advances in top-down fabrication techniques, hydrogel building blocks of various sizes, shapes, and compositions are readily designed to mimic architectures and interfaces observed in tissues *in vivo* (Du et al., 2011; Du et al., 2008; Li et al., 2011). Because cells are physically constrained within the building blocks, cell-laden hydrogels may be especially appropriate for studying the exchange of soluble factors between different cell populations (Scott et al., 2010) but are not appropriate for the study of juxtacrine or mechanically coupled cell-cell interactions such as those found in epithelium.

To study interactions between groups of cells that are physically connected, one could use modules made of cell aggregates without intervening ECM. Many tissues and organs (such as pancreatic islets, lymph nodes, and the lobules of the breast and liver) contain repetitive subunits consisting of groups of cells with dimensions of hundreds of microns to a millimeter. The majority of cells



within these repeating units are fully differentiated and structurally integrated with their neighbors. Multicellular aggregates of different shapes and sizes can be prepared using the same top-down techniques as those used for cell-laden hydrogel molding and similarly assembled into larger scale structures (Livoti and Morgan, 2010; Rago et al., 2009a; Rago et al., 2009b; Tejavibulya et al., 2011). Multicellular sheets can also be stacked to make multilayered structures (Haraguchi et al., 2012; Jean et al., 2011; Zahn et al., 2012). Preparing the aggregate building blocks before the assembly ensures that cells have fully formed cell-cell junctions. To date, the majority of these multicellular building blocks have been made using homogenous populations of cells. This assembly approach can thus result in heterogeneous interactions at the resolution of the interface between two building blocks containing different cell types, but is not precise enough to control interactions at the single cell level.

Directed assembly using cells as building blocks provides the fine resolution necessary for positioning single cells relative to each other to probe interactions between neighboring cells in a tissue. Not only are neighboring cells intimately physically and mechanically coupled, but neighboring cells also dynamically exchange soluble and non-soluble factors. Assembly at this fine level of spatial resolution is required for recreating stem cell niches (Losick et al., 2011) or when rebuilding cell-cell connections found in fully differentiated tissues (Desai et al., 2009). In specialized cases, cells have the ability to organize into desired structures at these length scales. Townes and Holtfreter famously found that dissociated cells from amphibian embryos would aggregate and self-sort into

germ layers without outside intervention (Townes and Holtfreter, 1955). This strategy occasionally allows a multiplicity of cell types to self-organize in wells or in hanging drops (Foty, 2011; Kunz-Schughart et al., 2006; Wenger et al., 2005), but in many cases isolated mixtures of cells do not spontaneously organize into structures that mimic their tissue of origin. In the absence of the necessary external positioning cues, directed assembly techniques can be used to spatially position cells in relation to each other at the microscale.

DNA-programmed assembly is a recently developed approach to direct the organization of multicellular structures *in vitro* with single-cell resolution (Gartner and Bertozzi, 2009) (Figure 1-3A-B). Key to this approach is the covalent or non-covalent remodeling of the adhesive properties of the cell surface with single-stranded DNA (ssDNA). Programmed cell assembly can also be achieved by labeling or binding other interacting biomolecules to cell surfaces, though these are often limited to only single pairs of interacting molecules (Dutta et al., 2011; Hamon et al., 2011; Liu et al., 2011; Zhao et al., 2011). Labeling different cell types with complementary strands or molecules can direct the formation of heterogeneous microtissues. Discrete multicellular architectures can be achieved by changing the ratios of labeled populations (Figure 1-3B-C). This strategy has been used to recapitulate synthetic paracrine signaling networks (Gartner and Bertozzi, 2009) and immune cell homing to sites of inflammation (Zhao et al., 2011).

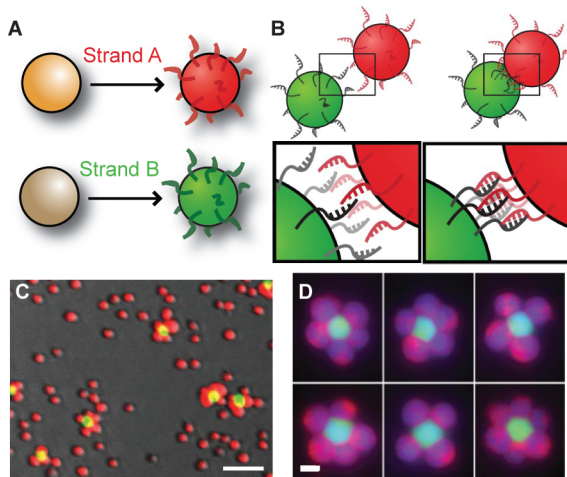


**FIGURE 1-3. DNA-templated programmed assembly method.** (A) Two populations of cells are stained with cytosolic dyes and labeled with complementary ssDNA sequences A and B. (B) The ssDNA on cell surfaces brings cells together through molecular recognition. (C) Cells stained with green and red cytosolic stains and labeled with complementary ssDNA are mixed 1-to-50. (Scale bars, 50  $\mu\text{m}$ ). (D) Enlarged images of discrete structures formed in 1-to-50 reactions. (Scale bars, 10  $\mu\text{m}$ ). Reproduced with permission from (Gartner and Bertozzi, 2009).

Programmed assembly of cellular building blocks can enable the study of close-range cell-cell interactions in controlled multicellular architectures. Since essentially any cell type can be labeled using the various DNA-labeling methods, and a nearly unlimited set of orthogonal DNA sequences are available, DNA-programmed assembly can be used to generate a variety of complex heterotypic cell-cell interactions for study. Importantly, the DNA used to program cellular interactions degrades rapidly at 37°C, and cells that are brought together using DNA-programmed assembly need not be genetically engineered (Hsiao et al., 2009; Selden et al., 2012). This technique closely apposes interacting cell surfaces and is ideally suited for the study of multicellular circuits that operate over short distances such as electrical and chemical signaling through gap junctions (Locke, 1998), short-range mechanical signaling coupled to the cytoskeleton (Eyckmans et al., 2011), juxtacrine signaling such as through the Notch pathway (Sprinzak et al., 2010), and short-range paracrine signaling such as through the Wnt and Hedgehog pathways.

## THREE-DIMENSIONAL CELL CULTURE

Tissue culture models using mammary epithelial cell lines have revealed many molecular aberrations that influence proliferative and invasive behaviors. The presence of soluble factors can be controlled in two-dimensional (2D) cell culture to mimic those found within the *in vivo* microenvironments. Additionally, genetic engineering and cell culture in standard 2D conditions have served to elucidate the role and mechanism of action of proteins such as the epidermal growth factor receptor (EGFR) ErbB2 in tumorigenesis. Unfortunately, other cell behaviors such as morphogenesis and tissue-level polarity are difficult to study when cells are grown on 2D tissue culture plastic. In these cases, a more complex culture set up is required.

3D epithelial culture models maintain cells into more *in vivo*-like microenvironments than the conditions of 2D culture systems. Increasing evidence in the past decade has also highlighted how the mechanical properties and dimensionality of the culture system can affect cell morphology and behavior (Baker and Chen, 2012; DuFort et al., 2011). In 3D culture, cells are grown in ECM-like materials that can be designed to mimic the elasticity, porosity, and presentation of bioactive molecules of the basement membrane adjacent to epithelial tissues in the human body. Both matrix composition and soluble factors can be manipulated under these conditions to study how signals displayed in a three-dimensional context affect cell behaviors.

As a result of these added features, 3D culture models have led to discoveries about cell and tissue behaviors that could not be made in a traditional culture format (Harari and Yarden, 2000). For instance, few differences in proliferation are discernable in 2D culture between the nonmalignant, spontaneously immortal HMT-3522 S1 breast epithelial cell line and its malignant derivative line HMT-3522 T4-2. When grown in laminin-rich ECM (lrECM) 3D culture, however, S1 cells form polarized, growth-arrested spheroids called acini while T4-2 cells grow into disorganized, tumor-like colonies with no growth arrest (Petersen *et al.*, 1992). These *in vitro* observations strongly parallel the observation that in nude mice, S1 cells are non-tumorigenic while T4-2 cells form invasive carcinomas (Briand *et al.*, 1996). MCF10A breast epithelial cells are another non-malignant model cell line that undergoes epithelial morphogenesis to form polarized microtissues that ultimately growth-arrest as multicellular acini under 3D culture conditions. Over-expression of ErbB2 leads to disruption of the morphogenesis in MCF10A cells and results in structures that mimic clinical features of ErbB2-driven breast cancer (Muthuswamy *et al.*, 2001). Because 3D culture results in small tissues that recapitulate important structural and functional features of the organ from which they were derived (Streuli *et al.*, 1991), we focused on designing a programmed assembly approach that interfaces with 3D culture conditions so that biologically relevant behaviors such as morphogenesis and tissue polarity could be observed.

In this work, we developed a DNA-templated programmed assembly approach to build mammary epithelial tissue models. This bottom-up strategy

allows us to design epithelial tissue models with single-cell resolution and is compatible with subsequent 3D culture. We applied this method for the study of homogeneous and heterogeneous cell-cell interactions that mimic those found in the human mammary gland.

## REFERENCES

Baker, B.M., and Chen, C.S. (2012). Deconstructing the third dimension: how 3D culture microenvironments alter cellular cues. *Journal of cell science* *125*, 3015-3024.

Correia, A.L., and Bissell, M.J. (2012). The tumor microenvironment is a dominant force in multidrug resistance. *Drug resistance updates : reviews and commentaries in antimicrobial and anticancer chemotherapy* *15*, 39-49.

DeNardo, D.G., Barreto, J.B., Andreu, P., Vasquez, L., Tawfik, D., Kolhatkar, N., and Coussens, L.M. (2009). CD4(+) T cells regulate pulmonary metastasis of mammary carcinomas by enhancing protumor properties of macrophages. *Cancer cell* *16*, 91-102.

Desai, R.A., Gao, L., Raghavan, S., Liu, W.F., and Chen, C.S. (2009). Cell polarity triggered by cell-cell adhesion via E-cadherin. *Journal of cell science* *122*, 905-911.

Du, Y., Ghodousi, M., Qi, H., Haas, N., Xiao, W., and Khademhosseini, A. (2011). Sequential assembly of cell-laden hydrogel constructs to engineer vascular-like microchannels. *Biotechnology and bioengineering* *108*, 1693-1703.

Du, Y., Lo, E., Ali, S., and Khademhosseini, A. (2008). Directed assembly of cell-laden microgels for fabrication of 3D tissue constructs. *Proceedings of the National Academy of Sciences of the United States of America* *105*, 9522-9527.

DuFort, C.C., Paszek, M.J., and Weaver, V.M. (2011). Balancing forces: architectural control of mechanotransduction. *Nature reviews Molecular cell biology* 12, 308-319.

Dutta, D., Pulsipher, A., Luo, W., and Yousaf, M.N. (2011). Synthetic chemoselective rewiring of cell surfaces: generation of three-dimensional tissue structures. *Journal of the American Chemical Society* 133, 8704-8713.

Eisenhoffer, G.T., Loftus, P.D., Yoshigi, M., Otsuna, H., Chien, C.B., Morcos, P.A., and Rosenblatt, J. (2012). Crowding induces live cell extrusion to maintain homeostatic cell numbers in epithelia. *Nature* 484, 546-549.

Elbert, D.L. (2011). Bottom-up tissue engineering. *Current opinion in biotechnology* 22, 674-680.

Engelhardt, J.J., Boldajipour, B., Beemiller, P., Pandurangi, P., Sorensen, C., Werb, Z., Egeblad, M., and Krummel, M.F. (2012). Marginating dendritic cells of the tumor microenvironment cross-present tumor antigens and stably engage tumor-specific T cells. *Cancer cell* 21, 402-417.

Eyckmans, J., Boudou, T., Yu, X., and Chen, C.S. (2011). A hitchhiker's guide to mechanobiology. *Developmental cell* 21, 35-47.

Foty, R. (2011). A simple hanging drop cell culture protocol for generation of 3D spheroids. *Journal of visualized experiments : JoVE*.



Gartner, Z.J., and Bertozzi, C.R. (2009). Programmed assembly of 3-dimensional microtissues with defined cellular connectivity. *Proceedings of the National Academy of Sciences of the United States of America* 106, 4606-4610.

Hamon, M., Ozawa, T., Montagne, K., Kojima, N., Ishii, R., Yamaguchi, S., Nagamune, T., Ushida, T., and Sakai, Y. (2011). Avidin-biotin-based approach to forming heterotypic cell clusters and cell sheets on a gas-permeable membrane. *Biofabrication* 3, 034111.

Haraguchi, Y., Shimizu, T., Sasagawa, T., Sekine, H., Sakaguchi, K., Kikuchi, T., Sekine, W., Sekiya, S., Yamato, M., Umezumi, M., *et al.* (2012). Fabrication of functional three-dimensional tissues by stacking cell sheets in vitro. *Nature protocols* 7, 850-858.

Hogan, C., Dupre-Crochet, S., Norman, M., Kajita, M., Zimmermann, C., Pelling, A.E., Piddini, E., Baena-Lopez, L.A., Vincent, J.P., Itoh, Y., *et al.* (2009). Characterization of the interface between normal and transformed epithelial cells. *Nature cell biology* 11, 460-467.

Hsiao, S.C., Shum, B.J., Onoe, H., Douglas, E.S., Gartner, Z.J., Mathies, R.A., Bertozzi, C.R., and Francis, M.B. (2009). Direct cell surface modification with DNA for the capture of primary cells and the investigation of myotube formation on defined patterns. *Langmuir : the ACS journal of surfaces and colloids* 25, 6985-6991.

Jean, J., Garcia-Perez, M.E., and Pouliot, R. (2011). Bioengineered Skin: The Self-Assembly Approach. *J Tissue Sci Eng* *S5*.

Johnston, L.A. (2009). Competitive interactions between cells: death, growth, and geography. *Science* *324*, 1679-1682.

Kunz-Schughart, L.A., Schroeder, J.A., Wondrak, M., van Rey, F., Lehle, K., Hofstaedter, F., and Wheatley, D.N. (2006). Potential of fibroblasts to regulate the formation of three-dimensional vessel-like structures from endothelial cells in vitro. *American journal of physiology Cell physiology* *290*, C1385-1398.

Leung, C.T., and Brugge, J.S. (2012). Outgrowth of single oncogene-expressing cells from suppressive epithelial environments. *Nature* *482*, 410-413.

Li, C.Y., Wood, D.K., Hsu, C.M., and Bhatia, S.N. (2011). DNA-templated assembly of droplet-derived PEG microtissues. *Lab on a chip* *11*, 2967-2975.

Liu, X., Yan, H., Liu, Y., and Chang, Y. (2011). Targeted cell-cell interactions by DNA nanoscaffold-templated multivalent bispecific aptamers. *Small* *7*, 1673-1682.

Livoti, C.M., and Morgan, J.R. (2010). Self-assembly and tissue fusion of toroid-shaped minimal building units. *Tissue engineering Part A* *16*, 2051-2061.

Locke, D. (1998). Gap junctions in normal and neoplastic mammary gland. *The Journal of pathology* *186*, 343-349.

Losick, V.P., Morris, L.X., Fox, D.T., and Spradling, A. (2011). *Drosophila* stem cell niches: a decade of discovery suggests a unified view of stem cell regulation. *Developmental cell* 21, 159-171.

Muthuswamy, S.K., Li, D., Lelievre, S., Bissell, M.J., and Brugge, J.S. (2001). ErbB2, but not ErbB1, reinitiates proliferation and induces luminal repopulation in epithelial acini. *Nature cell biology* 3, 785-792.

Ott, H.C., Matthiesen, T.S., Goh, S.K., Black, L.D., Kren, S.M., Netoff, T.I., and Taylor, D.A. (2008). Perfusion-decellularized matrix: using nature's platform to engineer a bioartificial heart. *Nature medicine* 14, 213-221.

Rago, A.P., Chai, P.R., and Morgan, J.R. (2009a). Encapsulated arrays of self-assembled microtissues: an alternative to spherical microcapsules. *Tissue engineering Part A* 15, 387-395.

Rago, A.P., Dean, D.M., and Morgan, J.R. (2009b). Controlling cell position in complex heterotypic 3D microtissues by tissue fusion. *Biotechnology and bioengineering* 102, 1231-1241.

Scott, E.A., Nichols, M.D., Kuntz-Willits, R., and Elbert, D.L. (2010). Modular scaffolds assembled around living cells using poly(ethylene glycol) microspheres with macroporation via a non-cytotoxic porogen. *Acta biomaterialia* 6, 29-38.

Selden, N.S., Todhunter, M.E., Jee, N.Y., Liu, J.S., Broaders, K.E., and Gartner, Z.J. (2012). Chemically programmed cell adhesion with membrane-anchored oligonucleotides. *Journal of the American Chemical Society* 134, 765-768.

Seliktar, D. (2012). Designing cell-compatible hydrogels for biomedical applications. *Science* 336, 1124-1128.

Sprinzak, D., Lakhanpal, A., Lebon, L., Santat, L.A., Fontes, M.E., Anderson, G.A., Garcia-Ojalvo, J., and Elowitz, M.B. (2010). Cis-interactions between Notch and Delta generate mutually exclusive signalling states. *Nature* 465, 86-90.

Streuli, C.H., Bailey, N., and Bissell, M.J. (1991). Control of mammary epithelial differentiation: basement membrane induces tissue-specific gene expression in the absence of cell-cell interaction and morphological polarity. *The Journal of cell biology* 115, 1383-1395.

Tejavibulya, N., Youssef, J., Bao, B., Ferruccio, T.M., and Morgan, J.R. (2011). Directed self-assembly of large scaffold-free multi-cellular honeycomb structures. *Biofabrication* 3, 034110.

Townes, P.L., and Holtfreter, J. (1955). Directed movement and selective adhesion of embryonic amphibian cells. *J Exp Zool* 128, 53-120.

Wenger, A., Kowalewski, N., Stahl, A., Mehlhorn, A.T., Schmal, H., Stark, G.B., and Finkenzeller, G. (2005). Development and characterization of a spheroidal coculture model of endothelial cells and fibroblasts for improving angiogenesis in tissue engineering. *Cells, tissues, organs* 181, 80-88.

Zahn, R., Thomasson, E., Guillaume-Gentil, O., Voros, J., and Zambelli, T. (2012). Ion-induced cell sheet detachment from standard cell culture surfaces coated with polyelectrolytes. *Biomaterials* 33, 3421-3427.

Zhao, W., Loh, W., Droujinine, I.A., Teo, W., Kumar, N., Schafer, S., Cui, C.H., Zhang, L., Sarkar, D., Karnik, R., *et al.* (2011). Mimicking the inflammatory cell adhesion cascade by nucleic acid aptamer programmed cell-cell interactions. FASEB journal : official publication of the Federation of American Societies for Experimental Biology 25, 3045-3056.



## **CHAPTER 2**

### ***PROGRAMMED ASSEMBLY OF EPITHELIAL MICROTISSUES***

Source: The following chapter was published in part from: Liu, J.S.; Farlow, J.T.; Paulson, A.; LaBarge, M.A.; Gartner, Z.J., 2012. Programmed Cell-to-Cell Variability in Ras Activity Triggers Emergent Behaviors during Mammary Epithelial Morphogenesis. *Cell Reports* 2, 1461-1470 and also contains unpublished data.

Contributions: I initiated the project and performed the majority of the experiments, with help from Justin Farlow. Zev Gartner and I wrote the manuscript with editorial input from all authors. I wrote the additional text in the Results (DNA-templated programmed assembly) and Discussion sections. Zev Gartner supervised the project.

## INTRODUCTION

The human breast is a complex organ that is built up from multiple cell types. The bilayered epithelium of the mammary gland has two principle building blocks: luminal epithelial cells (LEPs) and myoepithelial cells (MEPs) (Figure 2-1A). LEPs and MEPs play distinct functional roles, serving to secrete and pump milk, respectively. These cellular building blocks are organized into ducts and acini that are further supported by fibroblasts that synthesize and reside in a collagenous ECM. Endothelial cells provide additional support for these structures through a meshwork of capillaries delivering nutrients, (Figure 2-1B). Ducts and acini are further organized into terminal ductal lobular units (TDLUs) that are surrounded by a secondary and specialized ECM containing beds of adipocytes that add additional form to the organ (Figure 2-1C) (Tavassoli, 1999). Finally, TDLUs are organized into multiple lobes that drain into large ducts, together delivering milk to the nipple (Nelson and Bissell, 2006) (Figure 2-1D). Though the overall architecture of the gland is drastically remodeled over the course of a woman's lifetime, the relative position of the different cell types with respect to each other and the modular organization of the organ remain constant in healthy tissue.



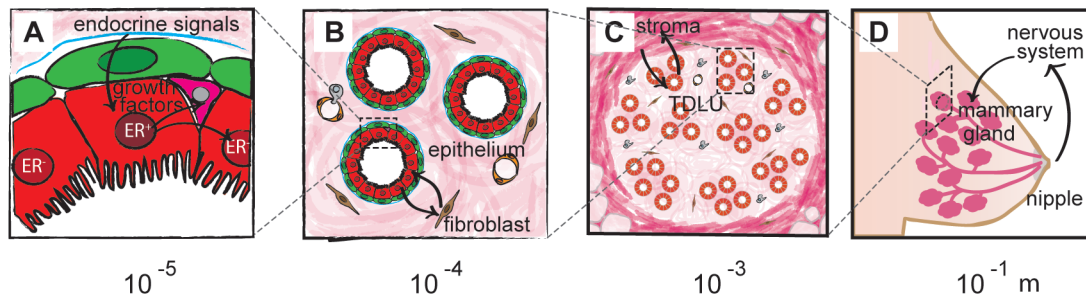


**FIGURE 2-1. The modular and hierarchical organization of the human mammary gland.** (A) Individual glandular epithelial cells exchange signals with each other and the basement membrane. (B) Epithelial cells of the ducts and acini also exchange signals with the surrounding lobular stroma. (C) Ducts and acini are organized into terminal ductal lobular units (TDLUs) that are embedded in a second type of collagenous ECM and that also contains many adipocytes. (D) The entire organ is integrated with the rest of the body to mediate its function in delivering milk during breast-feeding.

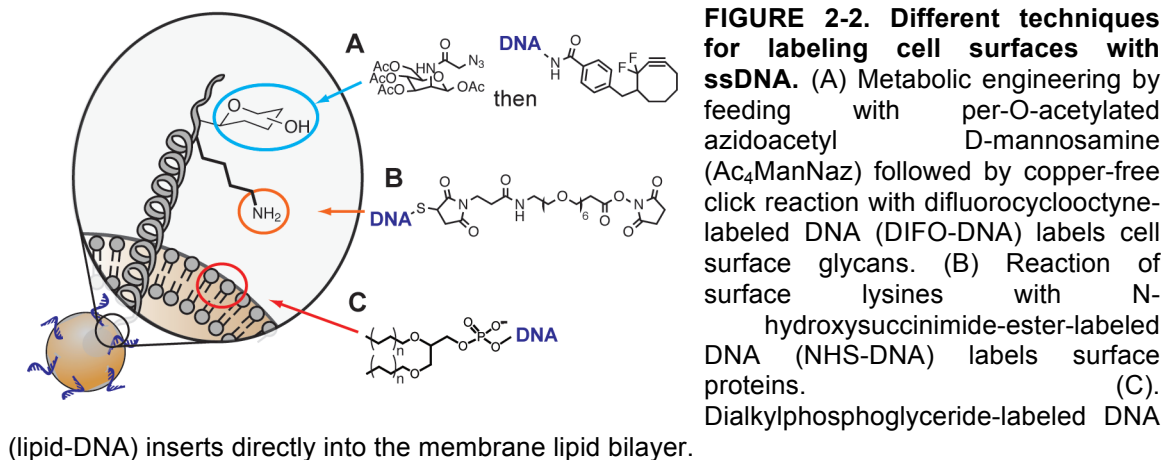
While the cell-type of origin for specific breast cancer subtypes remains an area of controversy, the majority of breast cancers are believed to originate from the LEPs that directly line the central, hollow lumen of mammary ducts and lobules (Petersen et al., 2001). In the disease state, many of the normal cell-cell signaling interactions between the LEPs and other cell types become dysregulated. These changes are exacerbated by tumor-associated fibroblasts that begin secreting factors that enhance cell migration and growth. The disrupted epithelium can also stimulate immune cell infiltration that can cause local inflammation. These processes drive a cycle of events that can disrupt the biochemical and structural homeostasis of the gland (Polyak and Kalluri, 2010). Locally, within the epithelial compartment of the mammary gland, non-transformed but cancer-associated MEPs and LEPs will often display biochemical changes (Allinen et al., 2004). The interaction with these neighboring epithelial cells is likely key in determining whether the malignant potential of a

mutant cell is suppressed or able to evade tissue surveillance mechanisms to proliferate and metastasize. Unfortunately, these early events in tumor progression are temporary and can also lead to disruption of the architecture of the mammary gland by the time the tissue is biopsied or resected for study. It is therefore difficult to monitor the *in vivo* sequence of biochemical or structural changes in the different epithelial cell populations of the tissue that must occur for cancer to progress.

To facilitate the study of cancer progression within the mammary gland epithelium, a tissue engineering approach such as DNA-templated programmed assembly has many advantages. The single cell resolution of DNA-templated programmed assembly is ideal for constructing simple epithelial structures that model the direct interactions between mutant and WT cells within the mammary epithelium. Precise control over the number and types of cell modules (i.e. healthy or diseased, LEP or MEP) incorporated in an engineered structure can allow for direct comparison of cell and tissue behaviors with different cellular components but within the same overall tissue architecture. DNA-templated programmed assembly may therefore segregate changes in tissue structure from changes in intrinsic cell characteristics. Programmed assembly could thus be a powerful tool to inform on the effects of pre-defined mutations in specific cell lineages on cancer-associated behaviors but requires the routine ability to assemble any mammary epithelial cell building blocks of our choosing.

Key to the successful application of DNA-templated programmed assembly is sufficient cell surface labeling with ssDNA. ssDNA can be introduced

to the cell surface by several means (Figure 2-2). In one approach, cells are first cultured in the presence of an azide-modified monosaccharide that is incorporated into cell surface glycans. The accessible azides can then react with a phosphine-conjugated ssDNA through Staudinger ligation or be coupled with a copper-free click reagent attached to ssDNA through [1,3]-dipolar cycloaddition reaction to covalently attach the DNA to the cell surface (Gartner and Bertozzi, 2009) (Figure 2-2A). N-hydroxysuccinimide-labeled DNA can also be covalently attached through reaction with free lysines on the cell surface (Hsiao et al., 2009) (Figure 2-2B). Lastly, lipid-conjugated DNA can passively partition into the cell membrane for surface modification (Borisenko et al., 2009; Liu et al., 2011; Selden et al., 2012; Teramura et al., 2010) (Figure 2-2C). This arsenal of labeling techniques increases the likelihood that at least one will sufficiently label any given cell type.



In this chapter, we focus on applying programmed assembly to model the epithelial compartment of the mammary gland. We describe the protocol used to

label model epithelial cell lines with ssDNA. We optimize conditions for lifting and labeling highly adherent epithelial cell lines and show that cells labeled with complementary strands can be assembled into homogeneous or heterogeneous aggregates. Finally, we demonstrate that purified, homogeneous assemblies of cell lines used in 3D culture systems form normal cell-cell adhesions and recapitulate key events of epithelial morphogenesis.

## RESULTS

### **DNA-TEMPLATED PROGRAMMED ASSEMBLY**

*Cell Labeling:* Programmed assembly has previously been used to build aggregates of 6–10 cells using suspension or loosely adherent cell lines (Gartner and Bertozzi, 2009). However, it was not known whether a similar protocol would label and direct the assembly of tightly adherent epithelial cells such as the MCF10A or Madin-Darby canine kidney (MDCK) lines. To prepare the single-cell suspensions of the adherent cell lines necessary for suspension-based programmed assembly, we first optimized for lifting conditions that yielded highly viable single cells but that also minimized trypsin exposure time to maintain surface levels of proteoglycans and proteins for subsequent labeling using strain-promoted click chemistry or amine acylation. We found that an incubation with EDTA in PBS without divalent cations initiated lifting of even highly adherent MCF10A and HMT3522 S1 cells, though viability decreased with incubation times over 30 minutes. We therefore pulsed the samples with trypsin for 30-60

seconds to complete the lifting and quenched the protease using soybean trypsin inhibitor. Any cells that remained attached to the culture dish could then be dislodged with 2% BSA in PBS without divalent cations. After removal from the culture substratum, cells could be washed either in the presence or absence of divalent cations, though viability and morphology were improved in buffers containing magnesium and calcium (data not shown).

To assay for labeling efficiency, we labeled cell suspensions with ssDNA using either the metabolic glycan engineering and copper-free click chemistry approach or the NHS-ester approach and then tested for the presence of the labeling strand using a fluorescent and complementary ssDNA probe. The extent of labeling of these samples was assessed using flow cytometry by determining the mean fluorescence increase (MFI) of DNA-labeled cells compared to unlabeled control cells. We also used beads with known numbers of fluorescent molecules to quantify the number of probe strands on the cells and compared these numbers to those on labeled Jurkat suspension cells, which had previously been shown to be sufficiently labeled for robust assembly (Gartner and Bertozzi, 2009). We found that we could achieve levels of surface labeling comparable to that of the Jurkat control cells for all epithelial cell lines tested using either the metabolic engineering and click chemistry approach or the NHS-ester approach (Figure 2-3A). The presence of surface ssDNA did not affect the proliferative capacity of these cell lines (Figure 2-3B). Robust labeling has also been achieved using the lipid-DNA method (Selden et al., 2012). Importantly, our panel

of tested epithelial lines included both non-malignant and malignant cell types, as well as model lines for both monolayered and bilayered structures.

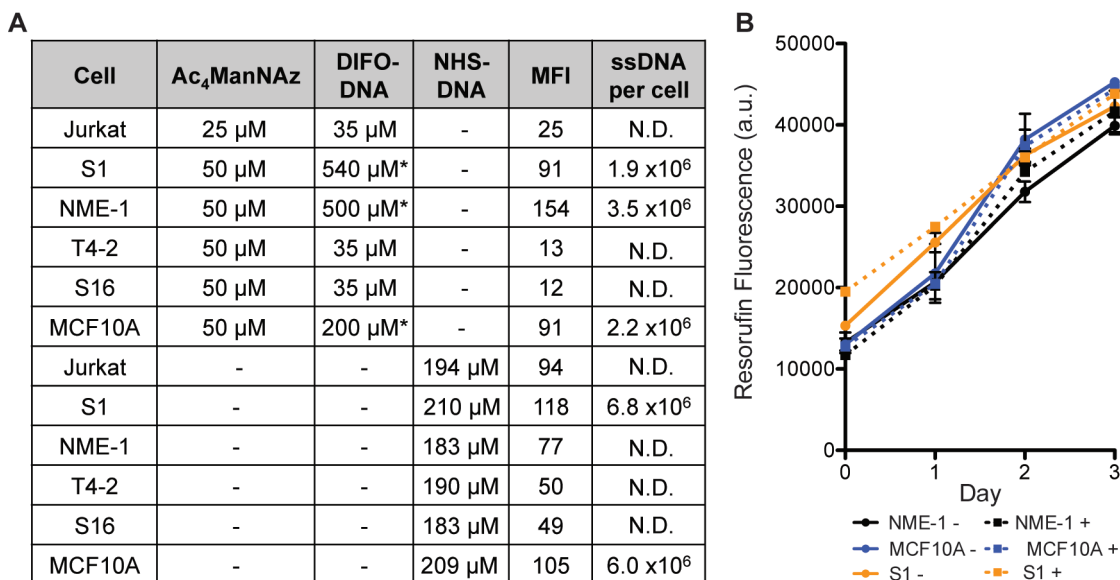


**FIGURE 2-3. ssDNA labeling in model breast epithelial cell lines.** (A) Table of mean fluorescence increases (MFI) and surface ssDNA quantification for a panel of breast cell lines with corresponding concentrations of reagents for either the metabolic engineering and click chemistry or the NHS-ester labeling approaches. (B) Proliferation of epithelial cell lines labeled with NHS-DNA (+) compared to unlabeled (-) controls. \* denotes samples labeled with a different batch of DIFO-DNA. (N.D., not done)

*DNA-templated cell assembly:* To confirm that the amount of ssDNA on epithelial cell surfaces was sufficient for programmed assembly, we assembled fluorescently marked cell populations labeled with complementary DNA strands. We assessed the extent of assembly using either microscopy or flow cytometry. When cells bearing complementary strands of ssDNA were assembled at a 1:1 ratio, large aggregates were observed rapidly after cell mixing. These aggregates contained equal amounts of red and green cells (Figure 2-4A) and could be made using either homogeneous or heterogeneous cell types (Figure 2-4B). No such aggregates were observed in reactions of cells labeled with mismatched

strands. When assembly reactions were performed with a 1:50 ratio of green to red cells, we observed more discrete structures with single green cells surrounded by 3-7 red neighbors (Figure 2-4C). These biased ratio assemblies could also be monitored on a flow cytometer and revealed that both homogeneous and heterogeneous structures could be made with greater than 80% efficiency (Figure 2-4D).

For downstream 3D culture and study, we next focused on isolating the discrete structures observed in the 1:50 ratio assemblies. Using fluorescently labeled cells and fluorescence activated cell sorting (FACS) at low pressure settings with a large 130  $\mu\text{m}$  nozzle, we could gate on double positive events and enrich for the assembled structures (Figure 2-4E). This step was integral for subsequent tracking and analysis of assemblies as it removed the majority of the single, unreacted cells. These one-step assemblies could also be sorted into another suspension of DNA-labeled cells to generate larger two-step assemblies that we enriched for using centrifugation, as these structures were too large for the nozzle sizes available on the cell sorter (Figure 2-4F).

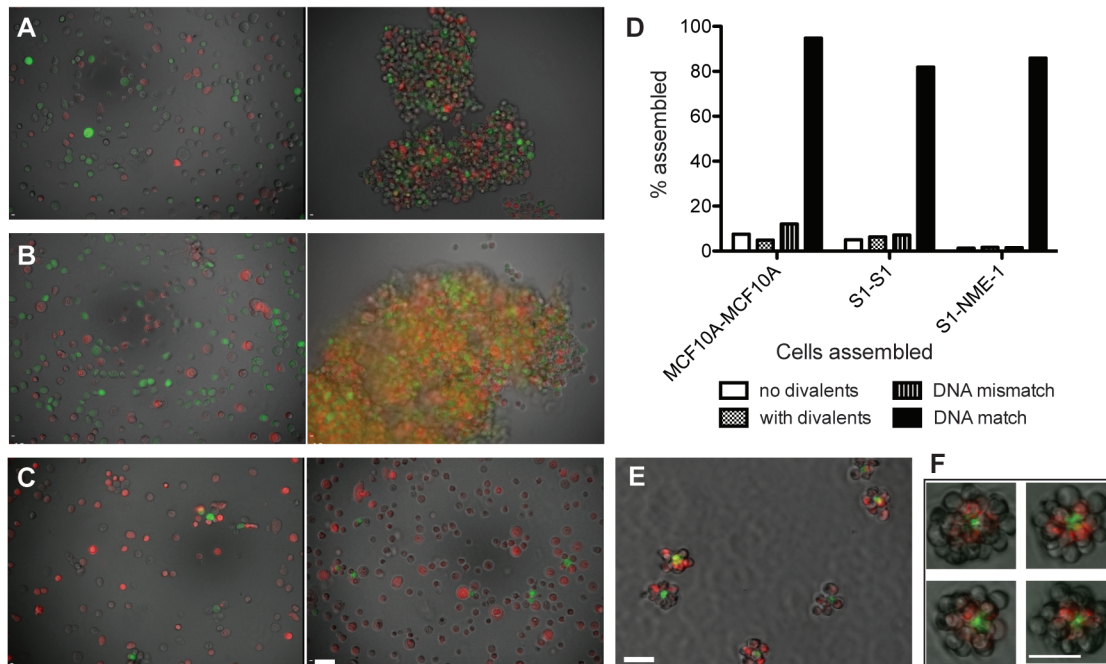


**FIGURE 2-4. Programmed assembly of homogeneous and heterogeneous structures.** (A) Homogeneous 1:1 assembly reactions of MCF10A cells stained with CellTracker dyes and labeled with either mismatched (left) or matched (right) NHS-DNA strands. (B) Heterogeneous 1:1 assembly reactions of metabolically engineered S1 cells (green) and NME-1 cells (red) stained with CellTracker dyes and labeled with either mismatched (left) or matched (right) DIFO-DNA strands. (C) 1:50 assembly reactions of homogeneous MCF10A (left) and heterogeneous S1-NME-1 cells (right). (D) Assembly efficiency graph of 1:50 assemblies determined by flow compared to unlabeled and mismatched control reactions. (E) Discrete structures purified from homogeneous 1:50 MCF10A assembly reactions using FACS. (F) Enlarged images of 2-step assemblies made by sorting single-step assemblies into a solution of unstained cells labeled with complementary ssDNA. (Scale bars, 50  $\mu$ m).

### 3D CULTURE OF HOMOGENEOUS MCF10A ASSEMBLIES

To ensure that the assembly and sorting process did not interfere with normal morphogenesis, we built homogeneous assemblies of MCF10A cells expressing H2B-fluorescent protein fusions and monitored their behaviors in 3D culture conditions (Figure 2-5A). One-step assemblies were purified and directly collected in chamber slide wells for on-top 3D culture (Lee et al., 2007). Assemblies that were thus sorted and cultured transitioned from aggregates of individual cells into spherical 3D microtissues with phase-dense boundaries over



6-12 hours (Figure 2-5B-C). Timelapse imaging of assemblies containing cells with fluorescently labeled nuclei revealed a transition from a disordered aggregate to a spherical microtissue with symmetrically arranged nuclei over a similar time frame (Figure 2-5D). Consistent with previous reports of MCF10A morphogenesis beginning from single cells, morphogenesis of microtissues formed by the programmed assembly process involved considerable cell motility (Ferrari et al., 2008; Pearson and Hunter, 2009; Tanner et al., 2012). These cell movements also became more concerted and continued at later time points (movie available online at *Cell Reports*).

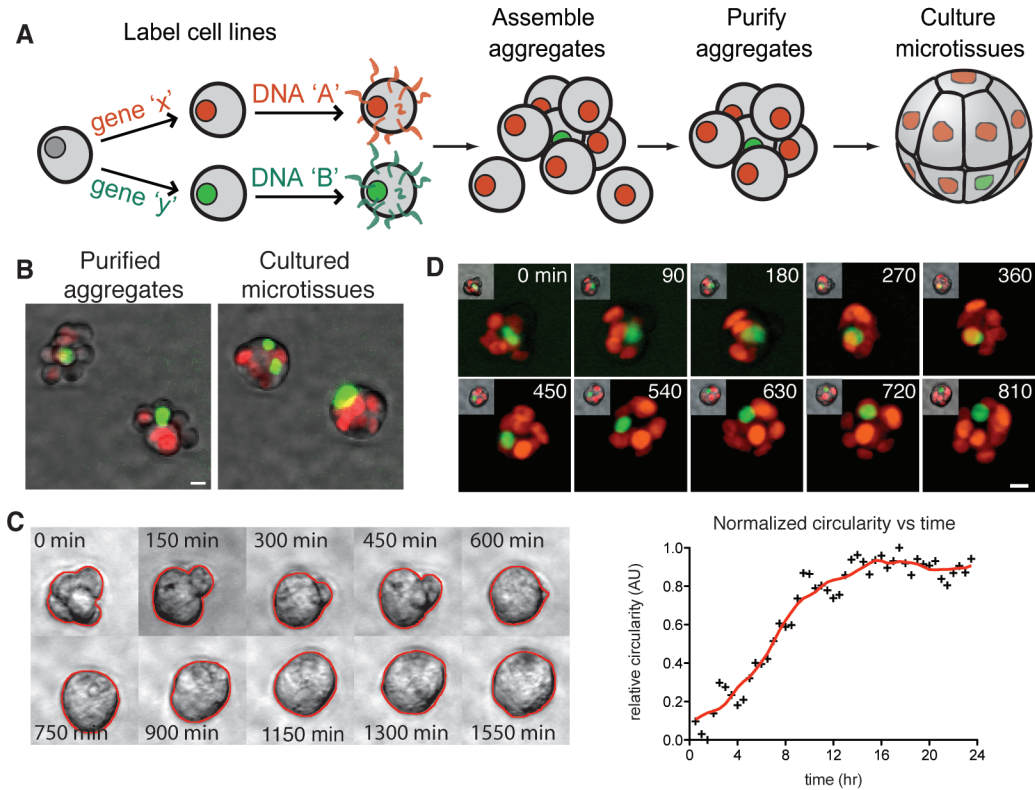


**FIGURE 2-5. Transfer of assembled aggregates into 3D culture.** (A) Scheme for the programmed assembly of mosaic epithelial microtissues. (B) MCF10A aggregates after purification by fluorescence activated cell sorting (left) condensed into rounded microtissues after 8.5 hr culture in IrECM (right). (C) Circularity of assembled aggregates in IrECM was assessed from the phase dark border of aggregates over time. Normalized average circularity was plotted by assigning a value of 1 to the average circularity at 24 hours, and 0 to the average circularity at time zero. The average value of 176 observations is plotted as a function of time. (D) Time series showing motion of fluorescently labeled nuclei during condensation of an aggregate (inset) into a microtissue. (Scale bar = 10  $\mu$ m).

The observation that multicellular aggregates are motile and rapidly condense suggested the cells were polarizing and replacing their DNA-based chemical adhesions with native-like, protein-based adhesions. To determine whether aggregates were indeed polarizing during the first 24 hours in culture, we performed indirect immunofluorescent staining for protein localization at regular intervals after programmed assembly and purification by FACS (Debnath et al., 2002). Immediately after sorting of MCF10A aggregates, hemidesmosomal

adhesion molecule  $\alpha_6$  integrin and adherens junction protein  $\beta$ -catenin were localized to individual cell edges, while cis-Golgi protein GM130 was randomly oriented relative to cell nuclei (Figure 2-6C and S1A). These results indicate that cells remained distinct entities immediately after programmed assembly despite their DNA-based chemical adhesions. By 12 hours post-assembly, these markers for cell polarity were enriched at appropriate subcellular locations (Figures 2-6C and S1A). By 24 hours protein localization was pronounced;  $\beta$ -catenin was enriched at cell-cell interfaces,  $\alpha_6$  integrin was enriched at the basolateral surface of the microtissue, and GM130 was apically localized relative to cell nuclei (Figures 2-6C and S1A). Additional staining of microtissues 24 hours post assembly revealed basal deposition of laminin-5 and actin enrichment at the cell cortex (Figure 2-6C). These staining patterns indicate that cell aggregates rapidly condense into polarized microtissues and are consistent with staining patterns of developing microtissues of similar size grown from single cells after 4 days in culture (Debnath et al., 2002) (Figures 2-6C and S1A). Polarity was also maintained at later timepoints (Figures 2-6D, S1B and S1C).

In addition to acquisition of tissue-level polarity, epithelial morphogenesis is marked by growth arrest followed by lumen formation after extended 3D culture (Debnath et al., 2002). Up to 96 hours post-assembly, the majority of assembled microtissues were uniformly positive for the proliferation marker Ki-67 (Figure 2-6D-E). However, microtissues were largely negative for Ki-67 at later time points. Moreover, cleaved caspase-3 in the clearing luminal space, which was largely absent at 24 hours, became evident as early as 96 hours and was

present in nearly all acini by day 16 (Figure 2-6D-E). These results indicate that polarized assembled aggregates develop into mature acini in 3D culture conditions.

To test the applicability of this approach for generating other epithelial microtissues, we evaluated the polarity and lumenogenesis of MDCK aggregates in 3D culture after programmed assembly. MDCK cells undergo lumenogenesis by a different mechanism than MCF10A cells, providing an additional test for the compatibility of programmed assembly with diverse cellular processes during morphogenesis. MDCK aggregates were assembled using lipid-DNA labeling and grown for 6-7 days in IrECM. Resulting cysts were uniformly polarized as judged by staining for apical marker gp135 and b-catenin (Figure 2-6F, left). Developing lumen were also observed in cysts, consistent with previous reports of MDCK cysts grown from aggregates (Liu et al., 2007). Additionally, the morphology of cysts was similar to the morphology of cysts of equivalent size grown from single cells (Figure 2-6F, right). Combined, these data indicate that the hallmarks of epithelial morphogenesis – polarity, growth arrest, and lumen formation – are recapitulated when epithelial cell aggregates prepared by programmed assembly are grown in 3D IrECM culture.

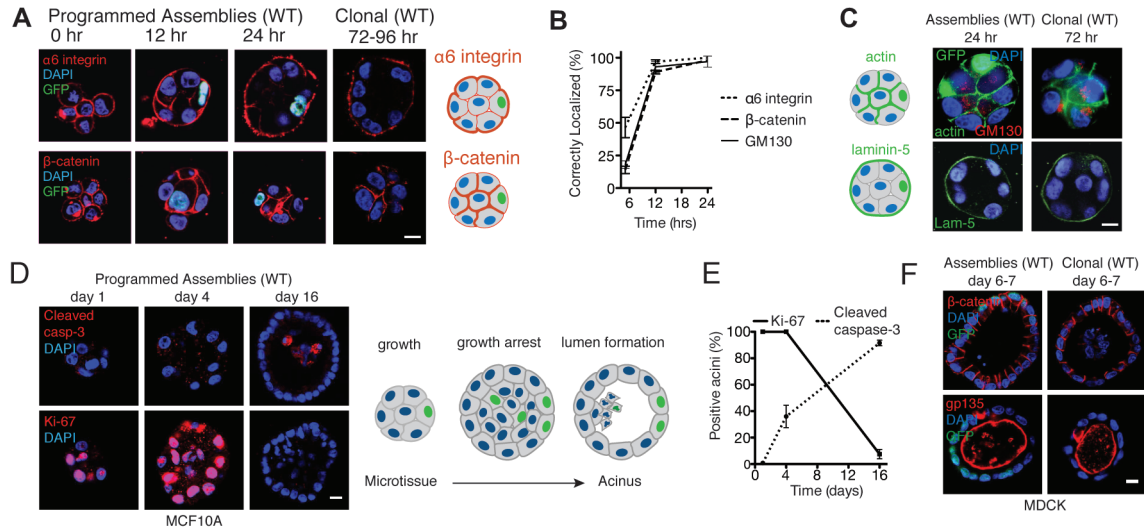


**FIGURE 2-6. Onset of polarity, growth arrest, and lumen formation in MCF10A cell aggregates.** (A) Representative confocal immunofluorescence images of MCF10A aggregates stained for  $\alpha_6$  integrin and  $\beta$ -catenin after 0, 12, and 24 hours in 3D culture, and representative immunofluorescence images of similarly sized microtissues grown from single cells for comparison (left). Schematic illustrating the correct localization of  $\alpha_6$  integrin and  $\beta$ -catenin for MCF10A microtissues undergoing morphogenesis (right). (B) Quantification of the onset of polarity in assembled aggregates of MCF10A<sup>WT</sup> cells. Values are means with error bars representing the standard deviations (SD) of the mean of 60 observations from at least two independent replicates. (C) Representative confocal immunofluorescence images of assembled MCF10A aggregates indicating correct localization of basement membrane component laminin-5 and cytoskeletal component F-actin after 24 hours in 3D culture. (D) Representative confocal immunofluorescence images of assembled MCF10A aggregates stained for cleaved caspase-3 and Ki-67 after 1, 4 and 16 days in culture (left). Schematic of MCF10A microtissue proliferation, growth arrest, and lumen formation (right). (E) Quantification of growth arrest and apoptotic lumen formation in microtissues grown from MCF10A aggregates. Data are expressed as the mean, and error bars represent the SD of the mean from at least two independent experiments (n = 60). (F) MDCK aggregates and similarly sized cysts grown from single cells stained for basolateral marker  $\beta$ -catenin and apical marker gp135 after 6 or 7 days. GFP indicates H2B-GFP-expressing cells in assemblies. (Scale bar, 10  $\mu$ m).

## DISCUSSION

In this chapter, we demonstrate the labeling of a variety of breast epithelial cell lines with ssDNA for programmed assembly. Cells can be labeled with one of three methods targeting different biomolecules on the cell surface, and cells are labeled with sufficient levels of ssDNA for robust assembly in suspension. By changing the stoichiometry of assembled cell populations and using fluorescently

labeled cells, we can build structures containing a seed cell surrounded by 3-7 neighboring cells and use FACS to enrich for these structures and for transfer to 3D culture conditions. We show that assemblies homogeneous for WT MCF10A or MDCK cells quickly condense into microtissues that undergo morphogenesis similar to microtissues grown from single cells, suggesting that the programmed assembly method does not interfere with normal epithelial morphogenesis.

Our results with homogeneous WT microtissues confirm that the programmed assembly method can be used to build controlled aggregates for 3D culture that develop into polarized colonies within 24 hours. Because the protocol is designed to be compatible with current 3D culture techniques, we could also manipulate culture factors, either soluble or insoluble, to determine which are necessary for multiple cells to recognize each other and form a polarized unit. Such studies might be useful for understanding which factors are required for injury repair and provide insight into the cellular behaviors required when damage to the epithelial layer is sensed, filled, and corrected. Assemblies similar to those presented here may also be useful building blocks in conjunction with other patterning techniques such as microcontact printing for building more complex constructs containing non-epithelial cell types distributed across larger length scales (Todhunter and Jee, unpublished data).

Using the assembly and purification protocol outlined, we can easily assemble multicellular structures containing two different cell populations with reproducible ratios (i.e. 1:6 or 6:1). Even these simple multicellular assemblies provide a powerful platform to study interactions between different cell types in

large numbers of identical structures in 3D culture. The next chapter outlines the application of this method to model a few types of heterotypic cell-cell interactions within the epithelium of the mammary gland.

## METHODS

### **CHEMICAL SYNTHESIS**

*Per-O-acetylated N-azidoacetyl D-mannosamine (Ac4ManNaz)*: Per-O-acetylated N-azidoacetyl D-mannosamine was synthesized as previously described (Saxon and Bertozzi, 2000). Synthetic schemes can be found in Appendix 1.

*Second-generation difluorocyclooctyne (DIFO)*: Second generation DIFO was synthesized as previously described (Codelli et al., 2008). Synthetic schemes can be found in Appendix 1.

*DNA and DNA-conjugates*: The following sequences were used for all labeling and assembly experiments:

**A:** 5'-ACTGACTGACTGACTGACTG-3'-C<sub>7</sub> NH<sub>2</sub>

**B:** 5'-CAGTCAGTCAGTCAGTCAGT-3'-C<sub>7</sub>-NH<sub>2</sub>

**Lipid DNA A:** 5'-dialkyl-(T)<sub>80</sub>-ACTGACTGACTGACTGACTG-3'

**Lipid DNA B:** 5'-dialkyl-(T)<sub>80</sub>-CAGTCAGTCAGTCAGTCAGT-3'

Oligonucleotides were synthesized on an Expedite 8909 using standard phosphoramidite chemistry. Phosphoramidites were purchased from Glen Research and AZCO biotech. Modified oligonucleotides were purified on an Agilent 1200 HPLC equipped with a semiprep Zorbax reversed phase C18 (oligos A and B) or semiprep Phenomenex C4 (Lipid DNA A and B) column and running a gradient of ACN in 0.1M TEAA from 8 to 80%. Purified oligonucleotides were extensively lyophilized prior to use.

DIFO-DNA was prepared by reacting amine-modified DNA with a PFP-ester of DIFO as previously described (Codelli et al., 2008). NHS-DNA was prepared by reacting thiol-modified DNA with NHS-PEG<sub>6</sub>-maleimide (Thermo) as previously described (Hsiao et al., 2009). Dialkylphosphoglyceride-DNA was prepared as previously described (Selden et al., 2012).

## **CELL CULTURE**

HMT3522 S1, HMT3522 T4-2, and HMT3909 S16 cells were kind gifts from Prof. Mina Bissell (Lawrence Berkeley National Labs) and grown in H14 media as previously described (Gudjonsson et al., 2002). NME-1 cells were also from Prof. Mina Bissell and grown in breast epithelial media (Lonza). MCF10A cells were kindly provided by Professor Jay Debnath (UCSF) and grown in DMEM/F12 media base with 5% horse serum (Invitrogen), 20 ng/mL EGF (Peprotech), 2 µg/mL hydrocortisone (Sigma), 10 µg/mL insulin (Sigma or Cell Applications), and 1 ng/mL cholera toxin (Sigma). MDCK cells were kindly provided by Professor Keith Mostov and cultured as previously described (Martin-Belmonte et



al., 2007) in MEM media supplemented with 10% fetal bovine serum and 1% antibiotics (all from UCSF Cell Culture facility).

## **LABELING OF CELL SURFACES**

*Metabolic engineering and DIFO-DNA approach:* HMT3522 S1 and NME-1 cells were grown in the presence of 50  $\mu\text{M}$  Ac<sub>4</sub>ManNAz for 3 days. For some experiments, cells were labeled with CellTracker dyes (Invitrogen) before lifting. These adherent cells were lifted by incubation in 0.04% EDTA until cells rounded (generally 10 minutes for NME-1, 20-30 minutes for S1, 15-20 minutes for MCF10A) followed by a 0.05% trypsin pulse for 30-50 seconds followed by quenching with soybean trypsin inhibitor (Sigma) in order to maintain levels of surface proteoglycans for subsequent DIFO-DNA labeling. Cells were washed 3 times with PBS without divalent cations and counted and then labeled with 50  $\mu\text{L}$  DIFO-DNA per  $10^6$  cells for 30 minutes at room temperature. Cells were then washed 3 times with reaction buffer (2% BSA in 1mM EDTA in PBS without divalent cations).

*N-hydroxysuccinimide-(PEG)6-labeled DNA approach:* Cells were lifted as above to maintain levels of surface proteins, resuspended in reaction buffer, and washed 3 times in serum-free base media. NHS-(PEG)<sub>6</sub>-DNA was prepared as described (Hsiao, et al., 2009). Cells were labeled with 50  $\mu\text{L}$  NHS-PEG6-DNA per  $10^6$  cells for 30 minutes at room temperature. Samples containing more than  $2 \times 10^6$  cells were agitated at least once during the labeling with pipetting to

ensure even labeling of cell surfaces. Cells were washed 3 times after labeling with serum-free base media before probe treatment or assembly.

*Dialkylphosphoglyceride-DNA approach:* Cells were lifted as above without the addition of soybean trypsin inhibitor and washed as in the NHS-DNA approach. Cells were labeled with 50  $\mu$ L dialkylphosphoglyceride-labeled DNA resuspended in PBS without divalent cations per  $10^6$  cells at room temperature on a tube shaker for 5-15 minutes.

### **QUANTIFICATION OF ssDNA ON SURFACES**

For labeling efficiency experiments, cells were incubated with FITC-conjugated complementary DNA for 15 minutes on ice, washed 3 times with reaction buffer, filtered through a 40  $\mu$ m mesh, and loaded onto a FACSCalibur flow cytometer for analysis. MESF beads (Bangs laboratories) were used to generate a standard curve for quantifying the number of FITC-conjugated strands on cell surfaces.

### **CELL PROLIFERATION ASSAY**

Cell proliferation was assessed using a resazurin reduction assay. Resazurin (Sigma) was incubated with cells (final concentration 0.1mg/mL) for 24 hours. The conversion of resazurin to resorufin was read on a Safire plate reader, and data were analyzed in Microsoft Excel.

## **ASSEMBLY EFFICIENCY AND PURIFICATION**

For crude cell assembly experiments, CellTracker- or H2B-FP- and DNA-labeled cells were filtered through a 40  $\mu\text{m}$  mesh, counted, and mixed at various ratios with a final cell concentration of  $10^6$  cells/mL in a 24-well plate. Assembly reactions were shaken on a plate shaker at 230rpm for at least 5 minutes before imaging on a Zeiss 200M inverted fluorescence microscope equipped with an XCite argon light source and a Hamamatsu camera. For assembly efficiency experiments, CellTracker-labeled cells were filtered, counted, mixed at greater than 1-to-50 ratios in SigmaCote-treated polystyrene tubes, centrifuged, and gently resuspended. Assembly efficiency was analyzed on a FACSCalibur. Using FACS, aggregates were purified directly into 8-chamber slides containing 3D assay media using a FACSArialII or FACSArialIII (UCSF Laboratory for Cell Analysis) equipped with a 130  $\mu\text{m}$  nozzle and a sheath pressure of 10 PSI.

## **3D CULTURE**

3D on-top cultures were performed as previously described in 3D culture media (2% Matrigel, 2% horse serum, 5 ng/mL EGF (Peprotech), 2  $\mu\text{g/mL}$  hydrocortisone, 10  $\mu\text{g/mL}$  insulin, and 1 ng/mL cholera toxin) using growth factor-reduced IrECM lots with protein concentrations between 9 and 11mg/mL (Matrigel, BD Biosciences) (Debnath et al., 2003). MDCK 3D culture was performed as previously described (Martin-Belmonte et al., 2007) in 2% Matrigel, 10% FBS, and 1% antibiotics in MEM media.

## **IMMUNOFLUORESCENCE STAINING AND CONFOCAL IMAGING**

3D cultures were stained as previously described (Debnath et al., 2003). The following antibodies were used for immunofluorescent staining: GM130,  $\beta$ -catenin (BD Biosciences),  $\alpha$ 6 integrin, laminin 5 (Millipore), cleaved caspase 3 (Cell Signaling), Ki-67 (Sigma), gp135 (a kind gift from Professor Keith Mostov), AlexaFluor488- and AlexaFluor568-conjugated goat anti-mouse, anti-rat, and anti-rabbit antibodies (Invitrogen). F-actin was stained with AlexaFluor488- or AlexaFluor568-conjugated phalloidin (Invitrogen). Confocal images were taken at the equatorial plane of the developing microtissues and were acquired on an inverted Zeiss LSM 510 NLO laser-scanning microscope (UCSF Laboratory for Cell Analysis). All imaged aggregates contained at least one GFP-labeled nucleus, although not necessarily in the plane of the confocal slice. Polarity, proliferation, and apoptosis counting were performed on a Nikon TiE inverted microscope equipped with a CSU-X1 confocal head. Channel intensities were adjusted linearly and equally across all images in each experiment using ImageJ and Adobe Photoshop software.

## REFERENCES

Allinen, M., Beroukhi, R., Cai, L., Brennan, C., Lahti-Domenici, J., Huang, H., Porter, D., Hu, M., Chin, L., Richardson, A., *et al.* (2004). Molecular characterization of the tumor microenvironment in breast cancer. *Cancer cell* 6, 17-32.

Borisenko, G.G., Zaitseva, M.A., Chuvilin, A.N., and Pozmogova, G.E. (2009). DNA modification of live cell surface. *Nucleic acids research* 37, e28.

Codelli, J.A., Baskin, J.M., Agard, N.J., and Bertozzi, C.R. (2008). Second-generation difluorinated cyclooctynes for copper-free click chemistry. *Journal of the American Chemical Society* 130, 11486-11493.

Debnath, J., Mills, K.R., Collins, N.L., Reginato, M.J., Muthuswamy, S.K., and Brugge, J.S. (2002). The role of apoptosis in creating and maintaining luminal space within normal and oncogene-expressing mammary acini. *Cell* 111, 29-40.

Debnath, J., Muthuswamy, S.K., and Brugge, J.S. (2003). Morphogenesis and oncogenesis of MCF-10A mammary epithelial acini grown in three-dimensional basement membrane cultures. *Methods* 30, 256-268.

Ferrari, A., Veligodskiy, A., Berge, U., Lucas, M.S., and Kroschewski, R. (2008). ROCK-mediated contractility, tight junctions and channels contribute to the conversion of a preapical patch into apical surface during isochoric lumen initiation. *Journal of cell science* 121, 3649-3663.

Gartner, Z.J., and Bertozzi, C.R. (2009). Programmed assembly of 3-dimensional microtissues with defined cellular connectivity. *Proceedings of the National Academy of Sciences of the United States of America* 106, 4606-4610.

Gudjonsson, T., Ronnov-Jessen, L., Villadsen, R., Rank, F., Bissell, M.J., and Petersen, O.W. (2002). Normal and tumor-derived myoepithelial cells differ in their ability to interact with luminal breast epithelial cells for polarity and basement membrane deposition. *Journal of cell science* 115, 39-50.

Hsiao, S.C., Shum, B.J., Onoe, H., Douglas, E.S., Gartner, Z.J., Mathies, R.A., Bertozzi, C.R., and Francis, M.B. (2009). Direct cell surface modification with DNA for the capture of primary cells and the investigation of myotube formation on defined patterns. *Langmuir : the ACS journal of surfaces and colloids* 25, 6985-6991.

Lee, G.Y., Kenny, P.A., Lee, E.H., and Bissell, M.J. (2007). Three-dimensional culture models of normal and malignant breast epithelial cells. *Nature methods* 4, 359-365.

Liu, H., Kwong, B., and Irvine, D.J. (2011). Membrane anchored immunostimulatory oligonucleotides for in vivo cell modification and localized immunotherapy. *Angew Chem Int Ed Engl* 50, 7052-7055.

Liu, K.D., Datta, A., Yu, W., Brakeman, P.R., Jou, T.S., Matthay, M.A., and Mostov, K.E. (2007). Rac1 is required for reorientation of polarity and lumen

formation through a PI 3-kinase-dependent pathway. *Am J Physiol Renal Physiol* 293, F1633-1640.

Martin-Belmonte, F., Gassama, A., Datta, A., Yu, W., Rescher, U., Gerke, V., and Mostov, K. (2007). PTEN-mediated apical segregation of phosphoinositides controls epithelial morphogenesis through Cdc42. *Cell* 128, 383-397.

Nelson, C.M., and Bissell, M.J. (2006). Of extracellular matrix, scaffolds, and signaling: tissue architecture regulates development, homeostasis, and cancer. *Annual review of cell and developmental biology* 22, 287-309.

Pearson, G.W., and Hunter, T. (2009). PI-3 kinase activity is necessary for ERK1/2-induced disruption of mammary epithelial architecture. *Breast cancer research : BCR* 11, R29.

Petersen, O.W., Lind Nielsen, H., Gudjonsson, T., Villadsen, R., Ronnov-Jessen, L., and Bissell, M.J. (2001). The plasticity of human breast carcinoma cells is more than epithelial to mesenchymal conversion. *Breast cancer research : BCR* 3, 213-217.

Polyak, K., and Kalluri, R. (2010). The role of the microenvironment in mammary gland development and cancer. *Cold Spring Harbor perspectives in biology* 2, a003244.

Saxon, E., and Bertozzi, C.R. (2000). Cell surface engineering by a modified Staudinger reaction. *Science* 287, 2007-2010.

Selden, N.S., Todhunter, M.E., Jee, N.Y., Liu, J.S., Broaders, K.E., and Gartner, Z.J. (2012). Chemically programmed cell adhesion with membrane-anchored oligonucleotides. *Journal of the American Chemical Society* 134, 765-768.

Tanner, K., Mori, H., Mroue, R., Bruni-Cardoso, A., and Bissell, M.J. (2012). Coherent angular motion in the establishment of multicellular architecture of glandular tissues. *Proceedings of the National Academy of Sciences of the United States of America* 109, 1973-1978.

Tavassoli, F.A. (1999). *Pathology of The Breast*, 2 edn (McGraw-Hill Professional).

Teramura, Y., Chen, H., Kawamoto, T., and Iwata, H. (2010). Control of cell attachment through polyDNA hybridization. *Biomaterials* 31, 2229-2235.



## **CHAPTER 3**

### **CONSEQUENCES OF CELL-TO-CELL VARIABILITY IN EPITHELIAL MICROTISSUES**

Source: The following chapter was published in part from: Liu, J.S.; Farlow, J.T.; Paulson, A.; LaBarge, M.A.; Gartner, Z.J., 2012. Programmed Cell-to-Cell Variability in Ras Activity Triggers Emergent Behaviors during Mammary Epithelial Morphogenesis. *Cell Reports* 2, 1461-1470.

Contributions: I initiated the project and performed the majority of the experiments, with help from Justin Farlow and Amanda Paulson. Zev Gartner and I wrote the manuscript with editorial input from all authors. I wrote the additional text in the Results (Suppression of proliferation mutants and Towards building bilayered structures) and Discussion sections. Zev Gartner and Mark LaBarge supervised the project.

## INTRODUCTION

Various levels of cell heterogeneity exist within the epithelium of the mammary gland, including signaling variability, differentiation variability, and morphological heterogeneity. Variability in signaling pathway activation between neighboring epithelial cells can arise from local differences in microenvironment, noisy gene expression, or acquired genetic or epigenetic changes. Many of these signals activate pathways downstream of the small GTPase Ras that affect behaviors including cell motility, survival, and proliferation. Previous studies have found that such cell-to-cell variability may lie dormant or trigger regulatory pathways that act at the level of cell communities to direct collective cell behaviors (Vitorino and Meyer, 2008), remove cellular defects from a tissue (Eisenhoffer et al., 2012; Takemura and Adachi-Yamada, 2011), or drive malignancy (Hogan et al., 2009; Leslie et al., 2010; Marusyk et al., 2012).

Though clonal MCF10A acini develop from a single cell, the activation levels of signaling pathways such as Ras signaling may differ between individual cells within the same multicellular structure over time. In the 3D MCF10A culture system, different levels of AKT phosphorylation have been observed across individual cells within clonal acini (Debnath et al., 2002). Similar cell-to-cell variability in levels of ERK and AKT phosphorylation has also been observed in primary breast tissue samples (LaBarge, unpublished data). Unfortunately, directly analyzing any functional consequences of such cell-to-cell variability in Ras pathway activation within 3D cultured or in vivo tissues has been

challenging, due in part to the difficulty of efficiently and selectively altering this signaling node in specific cells, within a growing microtissue, with both high temporal and spatial precision.

Another level of heterogeneity within the mammary gland exists between the luminal cells (LEPs) and myoepithelial cells (MEPs). *In vivo*, MEPs physically surround the LEP layer and secrete a basement membrane that separates the mammary epithelium from the stroma. Healthy MEPs have been termed “cellular tumor suppressors” in the past few decades due to their ability to inhibit the proliferation, invasion, and metastasis of cancer cells in 2D *in vitro* assays and in xenograft models (Polyak and Hu, 2005; Sternlicht *et al.*, 1997; Shao *et al.*, 1998; Jones *et al.*, 2003). Additionally, the inverted cellular polarity of acini derived from healthy, primary LEP cells when grown in 3D collagen matrices can be rescued on co-culture with healthy, primary MEPs (Gudjonsson *et al.*, 2002). These studies along with the observation that MEPs are largely absent in late stages of breast cancer (Petersen *et al.*, 2001) suggest that normal MEPs maintain a healthy mammary gland by providing microenvironmental cues to LEPs. It is unclear, however, whether this tumor suppressor ability is lost during breast cancer progression or whether it is diminished and misdirected due to tissue structure breakdown.

In some cases, healthy purified LEPs and MEPs can spontaneously self-organize *in vitro* into bilayered organizations when passively mixed and cultured under appropriate conditions. The uncontrolled mixing of cells, however, leads to a low efficiency of bilayered acinus formation in 3D culture, and only certain

combinations of normal MEPs and normal or cancerous LEPs spontaneously form acinar structures in a given matrix (Gudjonsson *et al.*, 2002; Holliday *et al.*, 2009). Because not all combinations of normal and cancerous MEPs and LEPs spontaneously assemble, a method for building acinar structures from arbitrary cell types is needed to better model early stages of breast cancer *in vitro*. Such a combinatorial approach could help outline the chronology of disease by indicating whether pre-cancerous LEPs induce changes in healthy MEPs, or whether disease-associated MEPs can cause aberrant behaviors in healthy or diseased LEPs.

An *in vitro* model that introduces targeted numbers of heterogeneous cells into an epithelium would be a useful platform for understanding how specific molecular mutations affect the behavior of neighboring cells and the overall tissue. Such heterogeneous epithelial tissue models can be prepared in a number of ways. Optogenetic techniques offer exceptional precision but are generally low throughput and require significant engineering of the protein or process of interest (Wang *et al.*, 2010). Currently, the best general solutions involve mixing two or more pre-defined cell populations (Mori *et al.*, 2009) or infection of tissues by low titer virus (Leslie *et al.*, 2010; Lu *et al.*, 2008). However, the resulting mosaic tissues span a distribution of compositions, where only a fraction of the microtissues possess the desired numbers of each cell type for subsequent analysis. These configurational inconsistencies complicate the quantification of rare events and processes that occur rapidly upon the initiation of cell-cell interactions.

In this chapter, we use programmed assembly as an alternative method for preparing epithelial microtissues of defined cellular composition for studying specific heterotypic cell-cell interactions. Control over the initial aggregate composition allowed us to build structures containing cells for either monolayered or bilayered acini. We use this approach to assemble MCF10A cells with modest relative differences in Ras pathway activation and demonstrate that specific patterns of cell-to-cell variability can induce emergent, tissue-level behaviors. We have also used a similar system to study the effect of proliferative advantages on cell survival within a multicellular acinus. Finally, we build assemblies with MEP-derived cell lines and study the potential of model cell lines to self-organize into bilayered structures in 3D culture.

## RESULTS

### **EMERGENT BEHAVIORS IN ASSEMBLIES WITH CONTROLLED CELL-TO-CELL VARIABILITY IN RAS PATHWAY ACTIVATION**

*MCF10A<sup>neoT</sup> (MCF10A<sup>Ras</sup>) cells undergo morphogenesis similar to MCF10A<sup>WT</sup> cells:* To understand how groups of cells undergoing morphogenesis respond to cell-to-cell variability in Ras activation within the same tissue, we required a MCF10A derivative cell with modestly elevated Ras activity, but also with basic epithelial character and the ability to interact with neighboring WT cells. Ras pathway activation in an ideal MCF10A derivative should be elevated but consistent with levels observed in normal tissues. However, we found that

cells expressing H-Ras<sup>V12</sup> under the control of strong viral promoters such as the pBabe-puro LTR had very high levels of Ras expression and Erk phosphorylation, lost E-cadherin expression and their epithelial morphology after a few passages, and formed highly invasive and disorganized structures in 3D culture (Figure 3-1B, S1D, and movies available online at *Cell Reports*) (Elenbaas et al., 2001). Therefore, MCF10A cells over-expressing H-Ras<sup>V12</sup> were a poor choice for modeling heterogeneous Ras activation during normal physiological processes.

In contrast, the MCF10AneoT cell line (referred to here as MCF10A<sup>Ras</sup> for clarity) retained its epithelial characteristics despite chronic H-Ras activation. These cells were generated by stable transfection of MCF10A with a constitutively active H-Ras<sup>V12</sup> gene (Basolo et al., 1991). Unlike acutely transduced cells, however, MCF10A<sup>Ras</sup> cells were previously shown to express only a modest 4-fold increase in H-Ras expression and a 3- to 6-fold increase in phospho-Akt relative to MCF10A<sup>WT</sup> (Kim et al., 2009). We confirmed these results and also observed a modest increase in phospho-ERK (Figure 3-1A). Additionally, MCF10A<sup>Ras</sup> cells were found to express nearly wild-type levels of E-cadherin (Figure 3-1A). Consistent with their modestly elevated H-Ras activity, MCF10A<sup>Ras</sup> cells formed acini that were larger in size than MCF10A<sup>WT</sup> acini but still lumenized when grown from single cells for 23 days in 3D culture (Figure 3-1B). Similar to MCF10A<sup>WT</sup> aggregates, assembled aggregates of MCF10A<sup>Ras</sup> cells condensed into polarized microtissues over 24 hours (Figure 3-1C and S1E). After 16 days in 3D culture they formed acini that were largely negative for Ki-67 but contained cells positive for cleaved caspase 3 in the lumen (Figures 3-

1D and S1F). We therefore used MCF10A<sup>Ras</sup> cells for building heterogeneous microtissues in subsequent experiments because they remained epithelial in character and displayed levels of Ras pathway activation consistent with normal tissues.

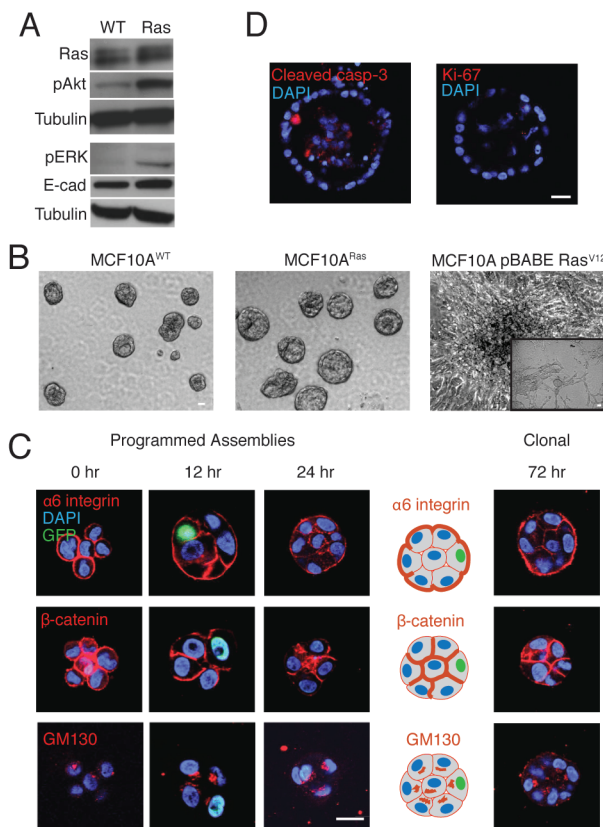


**FIGURE 3-1. Assembled MCF10ARas cells undergo morphogenesis similar to MCF10A WT cells.** (A) Western blots for expression of Ras, phospho-Akt, phospho-Erk and E-cadherin for MCF10A<sup>WT</sup> and MCF10A<sup>Ras</sup> cells. (B) Phase contrast images of MCF10A<sup>WT</sup>, MCF10A<sup>Ras</sup>, and pBabe-puro Ras<sup>V12</sup>-transduced MCF10A cells cultured for 23 days in IrECM. Inset shows the pBabe-puro Ras<sup>V12</sup>-transduced cells after 5 days of culture in IrECM. (C) Representative confocal immunofluorescence images of homogeneous MCF10A<sup>Ras</sup> cell aggregates stained for polarity and adherens junction proteins after culture in IrECM for the indicated times. These images should be compared to representative immunofluorescence images of similarly sized microtissues grown from single cells (right) and MCF10A<sup>WT</sup> staining patterns as shown in Figure 2A and S1A. (D) Representative confocal immunofluorescent images of homogeneous MCF10A<sup>Ras</sup> aggregates stained for cleaved caspase-3 and Ki-67 after 16+ days in culture. (Scale bars, 20  $\mu$ m).

*Single MCF10A<sup>Ras</sup> cells lead motile multicellular protrusions or basally extrude from WT microtissues:* Using programmed assembly, we prepared mosaic aggregates comprising a single MCF10A<sup>Ras</sup> cell surrounded by WT cells. While homogeneous aggregates of MCF10A<sup>Ras</sup> cells were phenotypically similar to WT aggregates with respect to polarity and morphology over 24 hours, we unexpectedly observed emergent phenotypes in heterogeneous microtissues. In

some cases, multicellular protrusions tipped by a single, motile MCF10A<sup>Ras</sup> cell seemed to direct the motion of the surrounding WT microtissue across the IrECM over several hours (Figure 3-2A, movies available online at *Cell Reports*). Multicellular protrusions occurred in 20-30% of the mosaic microtissues. In an additional 20-30% of mosaic aggregates, we observed cell extrusion where the single MCF10A<sup>Ras</sup> cell exited at the basal surface but remained loosely associated with the microtissue. Significantly, the multicellular protrusion and basal extrusion phenotypes were rarely observed for single MCF10A<sup>Ras</sup> cells grown within homogeneous MCF10A<sup>Ras</sup> microtissues (Figure 3-2B, movie available online at *Cell Reports*). Additionally, in 4-6% of the mosaic aggregates, the MCF10A<sup>Ras</sup> cell was highly motile and broke away from the surrounding WT microtissue, occasionally traversing over 100  $\mu\text{m}$  (Figures S2A, S2B and movie available online at *Cell Reports*). Addition of high activity DNase to the media immediately after sorting did not affect the frequency of extrusion and protrusions, indicating that DNA-based linkages between cells were not responsible for the observed phenotypes (Figure 3-2C). Protrusions and extrusions appear to be a result of single cells with elevated Ras activity as they were also observed in assemblies containing single cells expressing high levels of H-Ras<sup>V12</sup> under the pBabepuro LTR with WT neighbors (Figure S2C).



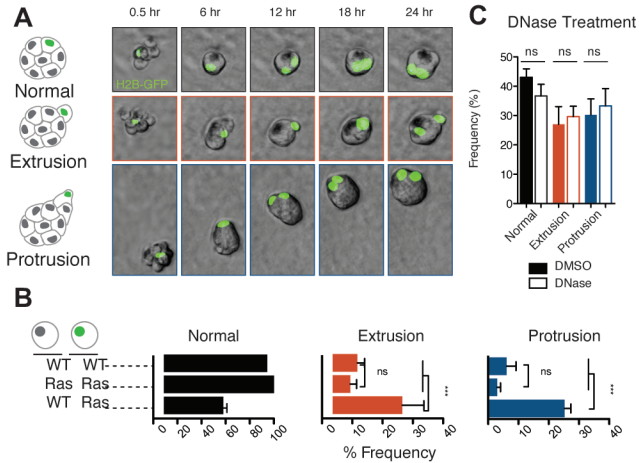


**FIGURE 3-2. Emergent behaviors in microtissues heterogeneous for signaling downstream of H-Ras.** (A) Representative timelapse images showing normal and emergent phenotypes in the mosaic MCF10A<sup>Ras</sup>/MCF10A<sup>WT</sup> microtissues. (B) Quantification of normal, basal cell extrusion, and motile multicellular protrusion frequency in homogeneous and heterogeneous microtissues. Data are expressed as the mean of at least 700 observations from 4 independent experiments, and error bars represent the SD of the mean. (C) Sensitivity of the frequency of emergent phenotypes to the addition of high activity DNase immediately after assembly.

Further characterization of heterogeneous microtissues revealed that both protruding and extruded cells were viable as judged by exclusion of a cell impermeant DNA stain (Figure 3-3A). Protruding cells were often irregularly shaped with GM130 staining oriented away from the microtissue center (Figure 3-3B-C) but with strong staining for  $\beta$ -catenin at cell-cell adhesions with neighboring WT cells (Figure 3-3D). Basally extruded cells typically maintained a rounded morphology. We did not observe an actin ring in adjacent cells or any unusual actin staining in extruded cells (Figure 3-3B). However, once fully extruded, cells did not exhibit  $\beta$ -catenin staining on membranes adjacent to the WT microtissue (Figure 3-3D). Since MCF10A<sup>WT</sup> and MCF10A<sup>Ras</sup> cells expressed similar levels of E-cadherin (Figure 3-2A) and were frequently observed to freely comingle, these behaviors could not be explained by differential E-cadherin expression alone (movies available online at *Cell Reports*). Moreover, heterogeneity, *per se*, was not responsible for the extrusion or multicellular protrusion phenotypes, as single WT cells did not protrude or extrude from

aggregates composed principally of MCF10A<sup>Ras</sup> cells (movie available online at *Cell Reports*).

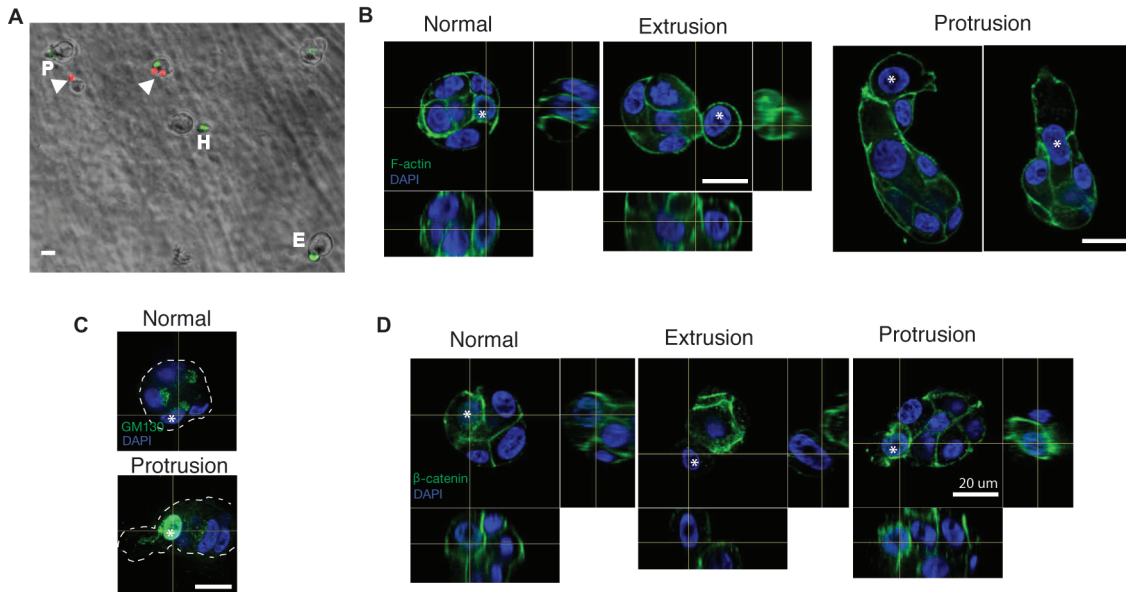


**FIGURE 3-3. Characterization of emergent behaviors by microscopy.** (A) Representative image of heterogeneous microtissues in DMSO-treated control treated with ethidium homodimer-1. Extruding (E), protruding (P), and hypermotile (H) cells are labeled and do not uptake ethidium homodimer. Arrowheads show other cells in the same field which have taken up ethidium homodimer. (B) Representative confocal immunofluorescence images of normal, basal extrusion, and motile multicellular protrusion phenotypes stained for F-actin. Orthogonal x-z and y-z planes are also shown. Samples were imaged for 12 hours prior to fixing and staining. The x-y coordinates of all microtissues manifesting emergent phenotypes were identified from the timelapse images. Motile multicellular protrusions and basal extrusions thus identified were relocated for imaging by confocal microscopy. (C) Representative confocal, immunofluorescence images of normal and protrusion phenotypes stained for GM130 after 12 hours in 3D culture as in B. The border of the microtissue is traced in dashed outline. (D) Representative confocal, immunofluorescence images of normal, basal extrusion, and motile multicellular protrusion phenotypes stained for  $\beta$ -catenin after 12 hours in 3D culture as in B and C. Asterisks mark H2B-GFP-expressing MCF10A<sup>Ras</sup> cells in (B), (C), and (D). (Scale bars, 20  $\mu$ m)

*Motility of MCF10<sup>Ras</sup> cells in homogeneous and heterogeneous microtissues is quantitatively different.* To further characterize the emergent behaviors resulting from heterogeneous Ras activity between cells during MCF10A morphogenesis, we tracked the positions of individual MCF10A<sup>WT</sup> or MCF10A<sup>Ras</sup>

cells in microtissues over 24 hours. MCF10A<sup>WT</sup> and MCF10A<sup>Ras</sup> cells did not differ significantly in maximum displacement from their initial positions when grown within homogeneous microtissues containing only cells of the same type (Figure 3-4A-B). This is consistent with the qualitative observation that homogeneous microtissues have a normal morphology over this time period. In contrast, the maximum displacement of single MCF10A<sup>Ras</sup> cells in heterogeneous aggregates with surrounding WT cells was increased relative to the same cells in homogeneous MCF10A<sup>Ras</sup> aggregates (Figure 3-4A-B) without a significant increase in average speed (Figure 3-4C). The increase in mean displacement of MCF10A<sup>Ras</sup> cells when grown among MCF10A<sup>WT</sup> cells was almost entirely attributable to microtissues with the multicellular protrusion phenotype (Figure 3-4D); when MCF10A<sup>Ras</sup> cell tracks were segregated into normal, extruding, and protruding phenotypes, we found average displacements ( $\pm$  95% CI) of 26 ( $\pm$  3), 31 ( $\pm$  5), and 61 ( $\pm$  9)  $\mu$ m, respectively. While the displacement of MCF10A<sup>Ras</sup> cells in normal and extruding microtissues typically remained within the average diameter of heterogeneous microtissues ( $43.7 \pm 8.47$   $\mu$ m, average diameter of 50 microtissues after 24 hours), the displacement of protruding cells generally exceeded the size of microtissues, sometimes significantly. To quantify the extent to which single, protruding MCF10A<sup>Ras</sup> cells affected the motility of the surrounding WT microtissue, we compared the trajectories of the MCF10A<sup>Ras</sup> cell to the trajectories of the overall microtissue. Overall, the trajectories for single MCF10A<sup>Ras</sup> cells and the surrounding WT microtissues were correlated for all three phenotypes (Figure S3). Interestingly, the large displacements observed for

single MCF10A<sup>Ras</sup> cells participating in motile multicellular protrusions were also observed for their associated WT microtissues (Figure 3-4E), indicating that the single MCF10A<sup>Ras</sup> cell does indeed direct the motion of the entire microtissue. Moreover, subtracting the coordinates of the microtissue centroid from the coordinates of the protruding MCF10A<sup>Ras</sup> cell generated residual trajectories (Figure 3-4E) that were qualitatively similar to those of single cells in homogeneous MCF10A<sup>Ras</sup> and WT microtissues (Figure 3-4A). This analysis occasionally revealed residual trajectories with large total displacements, which always corresponded to the rare, hypermotile cells (Figure 3-4E, dashed orange track).

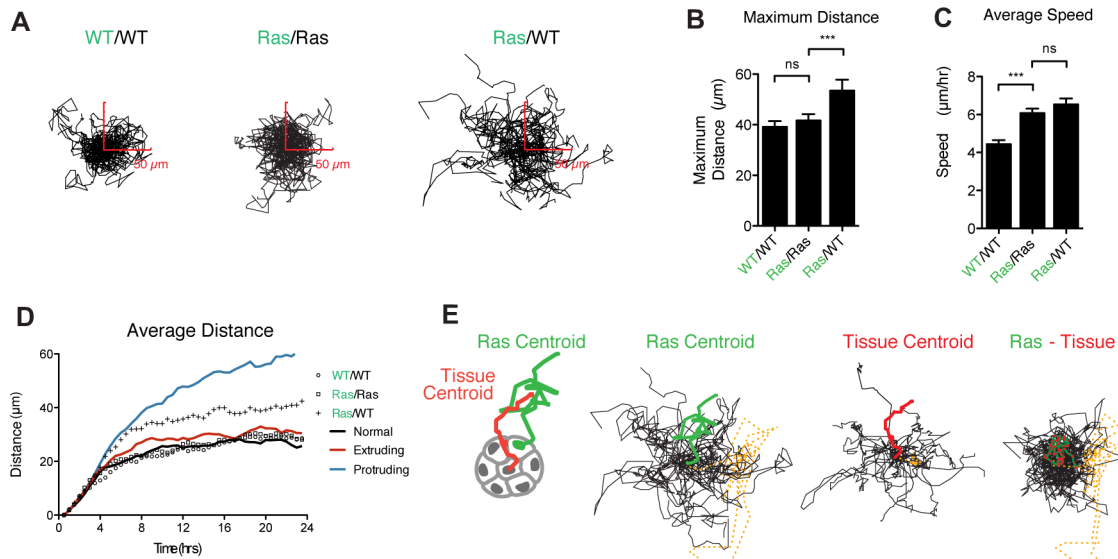


**FIGURE 3-4. Quantitative analysis of cell motility during emergent behaviors.** (A) Thirty superimposed 24-hour trajectories for cells expressing H2B-GFP fusions growing in homogeneous and heterogeneous MCF10A<sup>Ras</sup>/MCF10A<sup>WT</sup> microtissues. (B) Average maximum distance travelled and (C) speed of the H2B-GFP-expressing cell under the conditions in A. (D) Average distance travelled as a function of time for H2B-GFP-expressing cell in either homogeneous or heterogeneous microtissues. Average distances for H2B-GFP expressing cells in heterogeneous microtissues are broken down into normal, motile multicellular protrusion, and basal extrusion phenotypes. (E) Trajectories of H2B-GFP-expressing MCF10A<sup>Ras</sup> cells and the centroid of the surrounding WT microtissue. Microtissue trajectories (center) are subtracted from MCF10A<sup>Ras</sup> trajectories (left) to produce the residual trajectories (right). A representative MCF10A<sup>Ras</sup> cell (green), associated microtissue (red), and residual trajectory (hatched green and red) are highlighted. Trajectory of a hypermotile cell leaves a large residual (dashed orange lines). For (B) and (C), values are expressed as the mean with SD of 525 observations for 3 replicate experiments. For (A), (D) and (E), data are shown from a single experiment that is representative of 3 replicates.

## SUPPRESSION OF PROLIFERATION MUTANTS WITHIN MCF10A ACINI

Recent studies in polarized, growth-arrested, and lumenized MCF10A acini containing single mutant clones suggested that WT cells define a suppressive microenvironment in which mutant cells must be hyperproliferative, non-contact inhibited, and anti-apoptotic to propagate; mutant cells that are only hyperproliferative fail to exit the contact-inhibited WT environment (Leung and Brugge, 2012). We were curious whether the WT microenvironment would also

prevent mutant survival and proliferation in the context of a developing acinus, a proliferative microenvironment where the luminal space is not yet established. Such studies could serve as models for how mutant cells with proliferative oncogenes survive and spread in dynamic or actively remodeling epithelial tissues, such as during tissue repair or glandular expansion during menstrual cycles.

To determine how well a WT cellular microenvironment suppresses mutant cell survival in a developing acinus, we built assemblies containing single mutant cells surrounded by WT cells. The single inner cell was distinguished from the outer cells using different H2B-fluorescent protein fusions. The initial proliferative mutant used was a MCF10A line expressing HPV16 E7 protein (Debnath et al., 2002). We also built control assemblies homogeneous for either mutant E7 or WT cells as models for typical proliferation behaviors. Assemblies were followed by microscopy over 8 days in 3D culture (Figure 3-5A). Assemblies that had lost H2B-GFP-positive cells associated with the initial inner cell were counted at the 8-day end point as microenvironments that had suppressed mutant cell survival (Figure 3-5B). We found that single WT cells grown with WT neighbors were suppressed in 16% of acini counted, defining a background survival rate for single cells. In contrast to the findings in mature acini, we found that single E7 cells were less suppressed at 11% with WT neighbors in the developing microenvironment, indicating a survival advantage over WT cells. Surprisingly, E7 cells did not survive as well in homogeneous acini; 31% of day 8 structures had lost H2B-GFP-positive cells. Together, these findings indicate that

the mutant-suppressive cues of WT microenvironments in mature acini are not present during morphogenesis and that acini homogeneous for hyperproliferative cells may actually produce a more competitive microenvironment. In other words, survival during the early stages of morphogenesis may be determined at the level of relative proliferation rate alone.

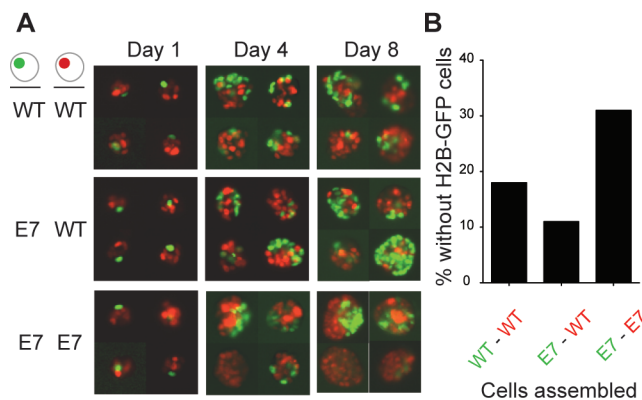


**FIGURE 3-5. Cell suppression in developing acini.** (A) Four representative assemblies with cells expressing H2B-FP fusion proteins were followed over the course of 8 days for each assembly type. (B) Suppression of H2B-GFP cells as determined by percent of assemblies that had lost GFP by day 8.

## TOWARDS BUILDING BILAYERED STRUCTURES USING PROGRAMMED ASSEMBLY

Since we had shown that a variety of cell lines derived from breast tissue could be labeled with ssDNA and assembled using programmed assembly, we could also in theory build aggregates containing myoepithelial cells and luminal epithelial cells capable of forming monolayered acini. To determine whether bringing these 2 cell types together in IrECM 3D culture conditions would be sufficient to promote *in vivo*-like organization, we built and cultured heterogeneous assemblies of HMT3522 S1 and NME-1 cells labeled with

CellTracker dyes (Figure 3-6A). Within a few days, the NME-1 cells quickly proliferated while the fluorescent signal of the S1 cells faded. The accelerated proliferation of NME-1 cells and the apparent death of S1 cells prevented the formation of a stable bilayered structure. From this study, we were unable to determine whether a stable structure would be possible with assemblies that incorporated more S1 cells or in structures with cells with matched proliferation rates.

To assess whether bilayered structures could be realized with cells that proliferate at more similar levels, we built heterogeneous assemblies with MCF10A and NME-1 cells as well (Figure 3-6B). These assemblies maintained both green- and red-labeled cells over the course of a few days. However, these two cell types also failed to form stable bilayered structures. They instead appeared to form mosaic structures with the 2 cell types adhering equally well to themselves as to each other. Together, the inability of these small heterogeneous aggregates to form bilayered structures suggests that these particular cell lines are not suitable models for the two cell types in the mammary gland.



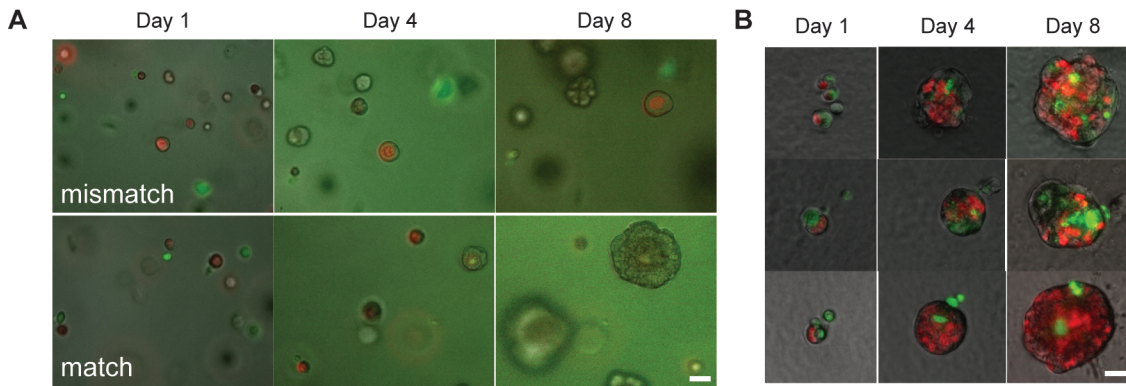


**FIGURE 3-6. 3D culture of heterogeneous assemblies containing NME-1 cells.** (A) Representative fields of CellTracker-labeled HMT3522 S1 (green) and NME-1 (red) cells assembled 1:1 and grown in embedded culture. Green fluorescence disappeared over 8 days. (B) Representative structures from assemblies containing MCF10A (CellTracker green) and NME-1 (H2B-RFP) cells in 3D on-top culture. (Scale bars, 20  $\mu$ m).

## DISCUSSION

In this chapter, we used programmed assembly to build a variety of heterogeneous cellular aggregates to mimic cell-cell interactions found in the mammary gland. Programmed assembly allowed us to directly investigate the consequences of cell-to-cell variability in Ras activation during the morphogenesis of MCF10A epithelial cells. Remarkably, we found that even subtle variability in Ras activation between neighboring cells elicits emergent behaviors during epithelial morphogenesis, including basal cell extrusions and motile multicellular protrusions. Epithelial cell extrusions that resemble those in our study are elicited under a variety of conditions. Cells over-expressing oncogenes such as ErbB2, Ras<sup>V12</sup> or v-Src have all been shown to extrude apically in confluent monolayer culture or growth-arrested mammary acini (Hogan et al., 2009; Kajita et al., 2009; Leung and Brugge, 2012). Cells undergoing apoptosis also extrude apically through the formation of a contractile

actin ring in the surrounding cells (Rosenblatt et al., 2001) or basally upon disruption of microtubule regulation (Slattum et al., 2009). Recently, apical cell extrusions were shown to occur as a consequence of cell crowding and proposed to contribute to tissue homeostasis (Eisenhoffer et al., 2012; Marinari et al., 2012). In this study, we observed the extrusion of single MCF10A<sup>Ras</sup> cells from within motile and growing MCF10A microtissues. In this dynamic 3D culture context, we found cell extrusions occurred in the basal direction and did not appear to occur through the formation of a contractile actin ring as occurs during apoptosis.

The simplest explanation for the observed basal, as opposed to apical, extrusions was that the polarized microtissues in our study lacked a well-defined and clear luminal space. The availability of an unobstructed basal surface lacking tissue culture plastic or a mature basement membrane may also provide an opportunity for basal extrusion that was lacking in previous studies. Similar conditions may exist during the morphogenesis of the mammary gland *in vivo* and at the basal surface of carcinomas of a variety of tissues (Gjorevski and Nelson, 2011). Alternatively, the increased constriction of the microtissues at the apical surface or differences between epithelial cell lines used in the various studies may also explain the differences in the direction of extrusion. In any case, in certain *in vivo* contexts, basal extrusions occur more frequently than apical extrusions (Hogan et al., 2009; Shen and Dahmann, 2005).

In addition to basal extrusions, we observed a high frequency of multicellular basal protrusions. Similar protrusions have previously been

observed during HGF-triggered tubulogenesis of MDCK cysts in 3D culture. HGF activates the Met receptor, which provides sustained activation of Ras similar to ectopic expression of H-Ras<sup>V12</sup> in our experiments (Khwaja et al., 1998; O'Brien et al., 2004). These behaviors may also play a role in angiogenesis and wound healing of endothelial cells (Graupera et al., 2008; Vitorino and Meyer, 2008). Motile multicellular protrusions are also analogous to border cell migration during *Drosophila* ovary development, where elevated growth factor receptor or Rac activation in single cells can drive collective cell motility of an entire cell aggregate (Inaki et al., 2012; Wang et al., 2010). Multicellular protrusions led by single cells may play a role during disease processes such as tumor progression and have been implicated in the invasive behaviors of cancers (Scott et al., 2010). While invasion by multiple transformed cells in these diseased contexts is a well-appreciated phenomenon, the observation that single cells expressing oncogenic H-Ras<sup>V12</sup> can drive the collective motility of non-transformed neighboring cells is surprising. Even more surprising is the fact that these multicellular protrusions, led by cells with only modestly elevated levels of activated Ras, are actually accentuated by the presence of neighbors with lower Ras activity. Similarly, we also observed an increased frequency of single MCF10A<sup>Ras</sup> cells breaking away from the surrounding microtissue and rapidly traversing hundreds of microns in 3D culture when surrounded by WT cells. These observations are consistent with a growing body of work that indicates tumor cell dissemination is an early event in carcinoma progression *in vivo* (Husemann et al., 2008; Rhim et al., 2012; Weinberg, 2008). Moreover, they

provide evidence that different modes of invasive behavior may coexist within the same tumor, where cellular heterogeneity is well documented (Friedl et al., 2012). Accordingly, our results may have significant implications for the initiation and progression of cancer.

In assemblies containing hyperproliferative MCF10A mutant cells expressing E7, we found that E7 mutant cells survived better with WT neighbors than with E7 neighbors. This is in contrast to previous reports indicating that cell proliferation is suppressed by WT cells in mature acini (Leung and Brugge, 2012). These previous studies implicated E-cadherin-based adhesions as the key cellular interaction in suppressing proliferation of mutant cells. Because E-cadherin localization to cell-cell junctions should be maintained in the acini in our studies (Debnath et al., 2002; Spancake et al., 1999), additional aspects of adherens junction signaling may be important for proliferation suppression. Future work may aim to address whether hyperproliferative neighbors hinder single mutant cell survival directly through cell-cell signaling effects or indirectly by monopolizing survival factors in the local microenvironment.

Our assembly platform may additionally be used to build assemblies containing cells with different mutations to determine whether certain hyperproliferative mutations are superior in survival capacity. Resistance to apoptosis is another mechanism for survival that can also be studied using this assembly approach. For example, use of cells that over-express Bcl2 may serve to determine whether cell survival can be increased with anti-apoptotic mutations especially during lumen formation when cells in the core of the acinus typically

undergo apoptosis (Debnath et al., 2002). Further analysis using confocal microscopy or flow cytometry analysis may also be used to better quantify the number of specific cell types within developing acini.

Finally, in our initial efforts to build a modular, *in vitro* model of the bilayered acinus, we found that even the nonmalignant model cell lines used were not capable of forming stable, bilayered structures. These cell lines have likely altered many native cell-cell and cell-ECM adhesion properties to adapt to propagation in 2D tissue culture conditions. The ability to self-organize has been demonstrated in primary human LEPs and MEPs, and may be retained in other breast epithelial cells that have had limited exposure to 2D cell culture conditions (Chanson et al., 2011). Using these alternative sources of cells in our programmed assembly approach may yield more *in vivo*-like structures. Additionally, other non-cellular factors such as media composition and ECM formulation may need to be optimized to direct the formation and stabilization of bilayered acini.

## METHODS

### **CELL CULTURE AND MATERIALS**

MCF10A, HMT3522 S1, and NME-1 cells were cultured as described in Chapter 2. MCF10AneoT cells were obtained from the Karmanos Cancer Institute (Detroit, MI) and cultured as previously described (Dawson et al., 1996; Debnath et al., 2003). Cell lines expressing H2B-RFP proteins were prepared by

transduction with lentivirus derived from pHIV-H2BmRFP (Addgene plasmid 18982) (Welm et al., 2008). H2B-eGFP was cloned from Addgene plasmid 11680 and ligated into pHIV to produce pHIV-eGFP (Kanda et al., 1998). Lentivirus was produced at the UCSF Sandler Lentiviral Core.

## **ANTIBODIES AND OTHER REAGENTS**

The following antibodies were used for Western blot: E-cadherin (BD Biosciences), tubulin (Sigma), phospho-Erk and phospho-Akt (Cell Signaling), pan-Ras (Calbiochem), goat anti-mouse-HRP, and goat anti-rabbit-HRP (Thermo). Ethidium homodimer-1 was purchased from Invitrogen and used at 1 $\mu$ M. Turbo DNase (Ambion) was used at a 1:200 dilution.

## **CELL LABELING, ASSEMBLY, AND 3D CULTURE**

Cell labeling using NHS-DNA, assembly, and assembly purification protocols are outlined in Chapter 1. 3D on-top cultures were performed as described in Chapter 1. 3D embedded cultures were performed as previously described. (Lee et al., 2007). For 3D culture of heterogeneous aggregates with cell types with different media formulations, a 1:1 mix of the medias was used.

## **MICROSCOPY**

Time-lapse images of aggregates were acquired on a Zeiss 200M inverted fluorescence microscope equipped with an XCite argon light source and a Hamamatsu camera. Field positions were programmed into Slidebook 5.0 software and images were acquired at 30-minute intervals. Samples were

maintained in a humidified chamber at 37°C and 5% CO<sub>2</sub>. Phenotypes were scored in Slidebook 5.0 software after acquisition. Microtissues that merged with other microtissues or single cells were not scored due to confounding effects on cell motility.

## **QUANTIFICATION OF BASAL EXTRUSION AND MULTICELLULAR PROTRUSION PHENOTYPES**

Apoptotic cells were excluded from phenotype quantification, as judged by cell morphology or uptake of ethidium homodimer-1 (Figure 3-3A). Extruding microtissues contained a single H2B-GFP-expressing cell pushed beyond the phase-bright boundary formed by the surrounding cells. Multicellular protrusions began with a single H2B-GFP-expressing cell that led the translation of the surrounding cells without becoming disconnected from the microtissue. H2B-GFP-expressing cells that broke away from tissues and moved alone were scored as protruding cells due to their altered morphology and motility.

## **CELL TRACKING AND TRAJECTORY ANALYSIS**

The center of the H2B-GFP nuclei in assemblies was tracked in Slidebook 5.0. Trajectories were exported and analyzed in Mathematica.

## **IMMUNOFLUORESCENCE STAINING AND CONFOCAL IMAGING**

3D cultures were stained and imaged as described in Chapter 2.

## REFERENCES

Basolo, F., Elliott, J., Tait, L., Chen, X.Q., Maloney, T., Russo, I.H., Pauley, R., Momiki, S., Caamano, J., Klein-Szanto, A.J., *et al.* (1991). Transformation of human breast epithelial cells by c-Ha-ras oncogene. *Molecular carcinogenesis* 4, 25-35.

Chanson, L., Brownfield, D., Garbe, J.C., Kuhn, I., Stampfer, M.R., Bissell, M.J., and LaBarge, M.A. (2011). Self-organization is a dynamic and lineage-intrinsic property of mammary epithelial cells. *Proceedings of the National Academy of Sciences of the United States of America* 108, 3264-3269.

Dawson, P.J., Wolman, S.R., Tait, L., Heppner, G.H., and Miller, F.R. (1996). MCF10AT: a model for the evolution of cancer from proliferative breast disease. *Am J Pathol* 148, 313-319.

Debnath, J., Mills, K.R., Collins, N.L., Reginato, M.J., Muthuswamy, S.K., and Brugge, J.S. (2002). The role of apoptosis in creating and maintaining luminal space within normal and oncogene-expressing mammary acini. *Cell* 111, 29-40.

Debnath, J., Muthuswamy, S.K., and Brugge, J.S. (2003). Morphogenesis and oncogenesis of MCF-10A mammary epithelial acini grown in three-dimensional basement membrane cultures. *Methods* 30, 256-268.

Eisenhoffer, G.T., Loftus, P.D., Yoshigi, M., Otsuna, H., Chien, C.B., Morcos, P.A., and Rosenblatt, J. (2012). Crowding induces live cell extrusion to maintain homeostatic cell numbers in epithelia. *Nature*.



Elenbaas, B., Spirio, L., Koerner, F., Fleming, M.D., Zimonjic, D.B., Donaher, J.L., Popescu, N.C., Hahn, W.C., and Weinberg, R.A. (2001). Human breast cancer cells generated by oncogenic transformation of primary mammary epithelial cells. *Genes & development* *15*, 50-65.

Friedl, P., Locker, J., Sahai, E., and Segall, J.E. (2012). Classifying collective cancer cell invasion. *Nature cell biology* *14*, 777-783.

Gjorevski, N., and Nelson, C.M. (2011). Integrated morphodynamic signalling of the mammary gland. *Nature reviews Molecular cell biology* *12*, 581-593.

Graupera, M., Guillermet-Guibert, J., Foukas, L.C., Phng, L.K., Cain, R.J., Salpekar, A., Pearce, W., Meek, S., Millan, J., Cutillas, P.R., *et al.* (2008). Angiogenesis selectively requires the p110alpha isoform of PI3K to control endothelial cell migration. *Nature* *453*, 662-666.

Hogan, C., Dupre-Crochet, S., Norman, M., Kajita, M., Zimmermann, C., Pelling, A.E., Piddini, E., Baena-Lopez, L.A., Vincent, J.P., Itoh, Y., *et al.* (2009). Characterization of the interface between normal and transformed epithelial cells. *Nature cell biology* *11*, 460-467.

Husemann, Y., Geigl, J.B., Schubert, F., Musiani, P., Meyer, M., Burghart, E., Forni, G., Eils, R., Fehm, T., Riethmuller, G., *et al.* (2008). Systemic spread is an early step in breast cancer. *Cancer cell* *13*, 58-68.

Inaki, M., Vishnu, S., Cliffe, A., and Rorth, P. (2012). Effective guidance of collective migration based on differences in cell states. *Proceedings of the National Academy of Sciences of the United States of America* 109, 2027-2032.

Kajita, M., Hogan, C., Harris, A.R., Dupre-Crochet, S., Itasaki, N., Kawakami, K., Charras, G., Tada, M., and Fujita, Y. (2009). Interaction with surrounding normal epithelial cells influences signalling pathways and behaviour of Src-transformed cells. *Journal of cell science* 123, 171-180.

Kanda, T., Sullivan, K.F., and Wahl, G.M. (1998). Histone-GFP fusion protein enables sensitive analysis of chromosome dynamics in living mammalian cells. *Current biology : CB* 8, 377-385.

Khawaja, A., Lehmann, K., Marte, M., and Downward, J. (1998). Phosphoinositide 3-Kinase Induces Scattering and Tubulogenesis in Epithelial Cells through a Novel Pathway. *J Biol Chem* 273, 18793-18801.

Kim, S.H., Miller, F.R., Tait, L., Zheng, J., and Novak, R.F. (2009). Proteomic and phosphoproteomic alterations in benign, premalignant and tumor human breast epithelial cells and xenograft lesions: biomarkers of progression. *International journal of cancer Journal international du cancer* 124, 2813-2828.

Lee, G.Y., Kenny, P.A., Lee, E.H., and Bissell, M.J. (2007). Three-dimensional culture models of normal and malignant breast epithelial cells. *Nature methods* 4, 359-365.

Leslie, K., Gao, S.P., Berishaj, M., Podsypanina, K., Ho, H., Ivashkiv, L., and Bromberg, J. (2010). Differential interleukin-6/Stat3 signaling as a function of cellular context mediates Ras-induced transformation. *Breast cancer research : BCR* 12, R80.

Leung, C.T., and Brugge, J.S. (2012). Outgrowth of single oncogene-expressing cells from suppressive epithelial environments. *Nature* 482, 410-413.

Lu, P., Ewald, A.J., Martin, G.R., and Werb, Z. (2008). Genetic mosaic analysis reveals FGF receptor 2 function in terminal end buds during mammary gland branching morphogenesis. *Developmental biology* 321, 77-87.

Marinari, E., Mehonic, A., Curran, S., Gale, J., Duke, T., and Baum, B. (2012). Live-cell delamination counterbalances epithelial growth to limit tissue overcrowding. *Nature* 484, 542-545.

Marusyk, A., Almendro, V., and Polyak, K. (2012). Intra-tumour heterogeneity: a looking glass for cancer? *Nature reviews Cancer* 12, 323-334.

Mori, H., Gjorevski, N., Inman, J.L., Bissell, M.J., and Nelson, C.M. (2009). Self-organization of engineered epithelial tubules by differential cellular motility. *Proceedings of the National Academy of Sciences of the United States of America* 106, 14890-14895.

O'Brien, L.E., Tang, K., Kats, E.S., Schutz-Geschwender, A., Lipschutz, J.H., and Mostov, K.E. (2004). ERK and MMPs sequentially regulate distinct stages of epithelial tubule development. *Developmental cell* 7, 21-32.

Petersen, O.W., Lind Nielsen, H., Gudjonsson, T., Villadsen, R., Ronnov-Jessen, L., and Bissell, M.J. (2001). The plasticity of human breast carcinoma cells is more than epithelial to mesenchymal conversion. *Breast cancer research : BCR* 3, 213-217.

Rhim, A.D., Mirek, E.T., Aiello, N.M., Maitra, A., Bailey, J.M., McAllister, F., Reichert, M., Beatty, G.L., Rustgi, A.K., Vonderheide, R.H., *et al.* (2012). EMT and dissemination precede pancreatic tumor formation. *Cell* 148, 349-361.

Rosenblatt, J., Raff, M.C., and Cramer, L.P. (2001). An epithelial cell destined for apoptosis signals its neighbors to extrude it by an actin- and myosin-dependent mechanism. *Current biology : CB* 11, 1847-1857.

Scott, R.W., Hooper, S., Crighton, D., Li, A., Konig, I., Munro, J., Trivier, E., Wickman, G., Morin, P., Croft, D.R., *et al.* (2010). LIM kinases are required for invasive path generation by tumor and tumor-associated stromal cells. *The Journal of cell biology* 191, 169-185.

Shen, J., and Dahmann, C. (2005). Extrusion of cells with inappropriate Dpp signaling from *Drosophila* wing disc epithelia. *Science* 307, 1789-1790.

Slattum, G., McGee, K.M., and Rosenblatt, J. (2009). P115 RhoGEF and microtubules decide the direction apoptotic cells extrude from an epithelium. *The Journal of cell biology* 186, 693-702.

Spancake, K.M., Anderson, C.B., Weaver, V.M., Matsunami, N., Bissell, M.J., and White, R.L. (1999). E7-transduced human breast epithelial cells show partial differentiation in three-dimensional culture. *Cancer research* 59, 6042-6045.

Takemura, M., and Adachi-Yamada, T. (2011). Repair responses to abnormalities in morphogen activity gradient. *Development, growth & differentiation* 53, 161-167.

Vitorino, P., and Meyer, T. (2008). Modular control of endothelial sheet migration. *Genes & development* 22, 3268-3281.

Wang, X., He, L., Wu, Y.I., Hahn, K.M., and Montell, D.J. (2010). Light-mediated activation reveals a key role for Rac in collective guidance of cell movement in vivo. *Nature cell biology* 12, 591-597.

Weinberg, R.A. (2008). Leaving home early: reexamination of the canonical models of tumor progression. *Cancer cell* 14, 283-284.

Welm, B.E., Dijkgraaf, G.J., Bledau, A.S., Welm, A.L., and Werb, Z. (2008). Lentiviral transduction of mammary stem cells for analysis of gene function during development and cancer. *Cell stem cell* 2, 90-102.



## **CHAPTER 4**

### **MOLECULAR CHARACTERIZATION OF RAS-DRIVEN EMERGENT BEHAVIORS**

Source: The following chapter was published in part from: Liu, J.S.; Farlow, J.T.; Paulson, A.; LaBarge, M.A.; Gartner, Z.J., 2012. Programmed Cell-to-Cell Variability in Ras Activity Triggers Emergent Behaviors during Mammary Epithelial Morphogenesis. *Cell Reports* 2, 1461-1470 but is mostly preliminary, unpublished data.

Contributions: I initiated the project and performed experiments. Zev Gartner and I wrote the manuscript with editorial input from all authors. I wrote the additional text in the Results (all sub-sections) and Discussion sections. Zev Gartner supervised the project.

## INTRODUCTION

Our observation that single epithelial cells expressing low levels of activated Ras display emergent behaviors when growing alongside WT neighbors was intriguing in light of the WT-like behavior of assemblies homogeneous for Ras-expressing cells. This observation suggests that the behavior of single cells within these cellular communities is context-dependent and that cells are capable of detecting differences in signaling states between themselves and their neighbors. It is unclear, however, what molecular signals transmit these differences from cell to cell or how these signals differ in microtissues undergoing cell extrusion, cell protrusion, or normal morphogenesis.

A number of mechanisms may explain the incidence of the emergent behaviors. Ras activates a number of downstream pathways in its GTP-bound state, most significantly the PI3K/AKT and MAPK pathways. Since MCF10A<sup>Ras</sup> cells express a constitutively active Ras molecule, the elevated basal activity of PI3K and MAPK signaling pathways are likely candidates for pathways involved in the emergent extrusion and protrusion phenotypes. MCF10A cells transformed with Ras have also been shown to upregulate the secretion of cytokines and growth factors such as IL-6 and TGF $\beta$ 1 (Leslie et al., 2010; Wang et al., 2010); such molecules may drive local autocrine or paracrine loops that cause extrusions and protrusions. Ras activation also triggers changes in the sensitivities of growth factor receptors to these autocrine and paracrine signals, providing a possible mechanism for the differential behavior of MCF10A<sup>Ras</sup> cells



in WT and mutant microenvironments (Young et al., 2013). Finally, Ras transformation can also affect cell adhesion machinery in MCF10A cells (Kinch et al., 1995). It is possible that adhesion or cohesion defects in MCF10A<sup>Ras</sup> cells only elicit changes to cellular behavior in the context of MCF10A<sup>WT</sup> cells (Steinberg, 1963).

In this chapter, we begin to explore these molecular mechanisms that may be involved in orchestrating the emergent behaviors observed in MCF10A microtissues with cell-to-cell variability in Ras pathway activation. We use a variety of techniques including pathway-specific, small-molecule inhibition, neutralizing antibody treatment, targeted RNA interference, and clonal isolation to investigate the putative role of a panel of signaling molecules. Our findings indicate that extrusions and protrusions have differential dependencies on signaling effectors downstream of Ras as well as other cell communication mechanisms including cadherin-based adhesion and paracrine signaling pathways such as TGF $\beta$ .

## RESULTS

### **INHIBITION OF EFFECTORS DOWNSTREAM OF RAS**

To investigate the molecular players that might be involved in the emergent phenotypes, we looked for changes in phenotype frequency in heterogeneous assemblies on treatment with small-molecule inhibitors of kinases

downstream of Ras signaling. Ras activates multiple pathways in its GTP-bound form. PI3K and the MAPK signaling cascades have recently been implicated as important downstream effectors of analogous protrusive membrane activity and apical cell extrusions, respectively, during H-Ras<sup>V12</sup> over-expression in confluent 2D MDCK monolayers and model organisms (Hogan et al., 2009). To determine whether these pathways were also necessary for basal cell extrusion and motile multicellular protrusions during heterogeneous MCF10A aggregate morphogenesis in IrECM, we treated freshly assembled mosaic aggregates with small-molecule inhibitors and quantified the distribution of resulting phenotypes over 24 hours in culture. Treatment with PI3K inhibitor LY294002 or PIK-90 reduced the formation of multicellular protrusions while slightly increasing the frequency of basal extrusions compared to treatment with DMSO control (Figures 4-1A-C). In contrast, treatment of mosaic aggregates with the MEK-inhibitor PD325901 or the Raf-inhibitor Sorafenib blocked both multicellular protrusions and basal extrusions (Figures 4-1A-C). The morphology of aggregates treated with inhibitors was indistinguishable from those treated with DMSO vehicle control (Figure 4-1D-E). Therefore, MEK activation was required for basal extrusions, whereas both PI3K and MAPK signaling pathways were necessary for motile multicellular protrusions.

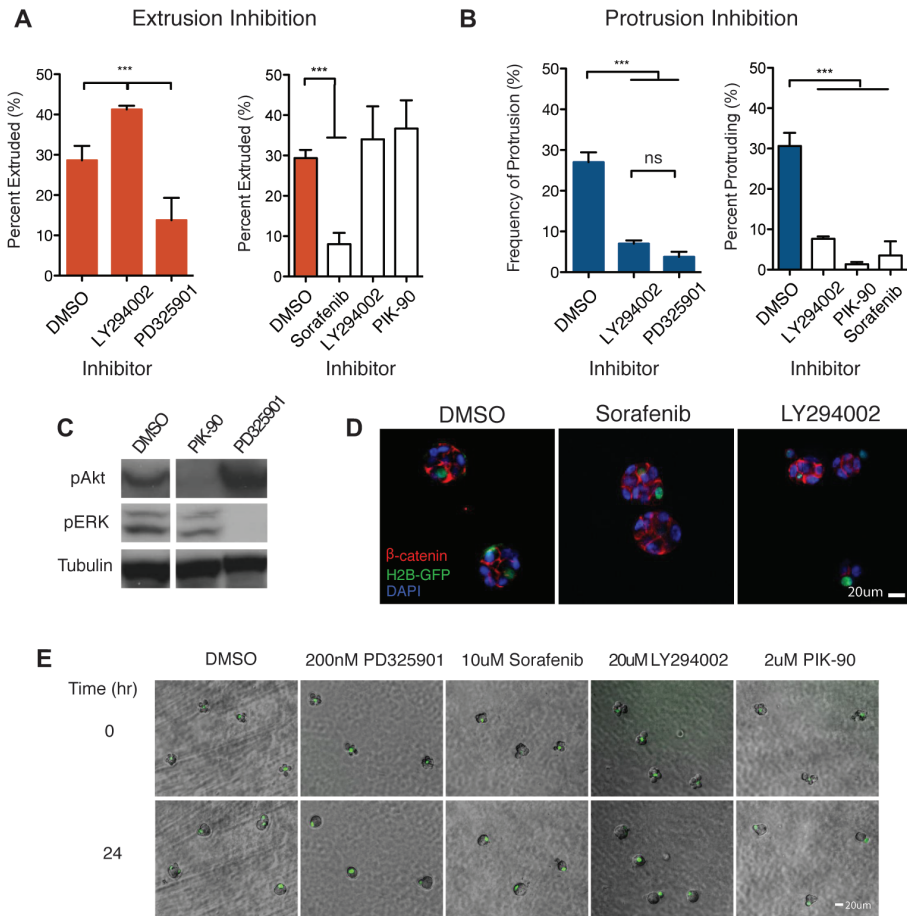


**FIGURE 4-1. Treatment of emergent phenotypes with small-molecule inhibitors of Ras effectors.** (A) Sensitivity of cell extrusion and (B) motile multicellular protrusions to inhibition of PI3K by LY294002 and PIK-90, and MEK by PD325901 or Raf by Sorafenib. Values are the averages of at least 400 total events from 3 independent experiments, and error bars show the SD of the means. \*\*\* = ( $p < 0.001$ ); ns = not significant (1-way ANOVA and Tukey's test). (C) Western blot of phospho-ERK and phospho-Akt Ser473 in MCF10A<sup>Ras</sup> cells treated with PIK-90 or PD325901. (D) Representative confocal, immunofluorescence images of heterogeneous MCF10A<sup>Ras</sup> /MCF10A<sup>WT</sup> aggregates treated with LY294002 or Sorafenib after 24 hours in 3D culture and then stained for  $\beta$ -catenin. (E) Representative phase contrast images of heterogeneous MCF10A<sup>Ras</sup> /MCF10A<sup>WT</sup> aggregates treated with kinase inhibitors after 0 and 24 hours in 3D culture. (Scale bars, 20  $\mu$ m).

Treatment of assembled aggregates with inhibitors resulted in inhibition of kinase activity in both cell populations, but relative differences in Ras activity across the microtissue are necessary to elicit cell extrusions and protrusions. We were curious whether corresponding differences in PI3K and MEK pathway

activation were required between Ras-expressing and WT cells for extrusions and protrusions. Towards addressing this question, we began by exploring RNA interference as a tool to differentially block signaling in one or the other cell population in our assay. We initially looked at MEK1 as a candidate, as the MEK/ERK pathway has been previously shown to induce cell motility in mature MCF10A acini (Pearson and Hunter, 2009). We used pools of double-stranded RNA molecules targeting MEK1 to knock down the expression of MEK1 protein in either MCF10A<sup>WT</sup>, MCF10A<sup>Ras</sup>, or both cells (Figure 4-2A). Heterogeneous assemblies where MEK1 was knocked down in both cell types did not affect the distribution of phenotypes compared to assemblies in which cells were treated with a scrambled siRNA control (Figure 4-2B). Further experiments are needed to determine whether this lack of effects on the emergent behaviors is due to incomplete MEK1 knockdown. Additionally, since some redundancy exists between MEK1 and MEK2, combinations of RNAi towards both may be required to block the functional consequences of MAPK signaling (Voisin et al., 2008).

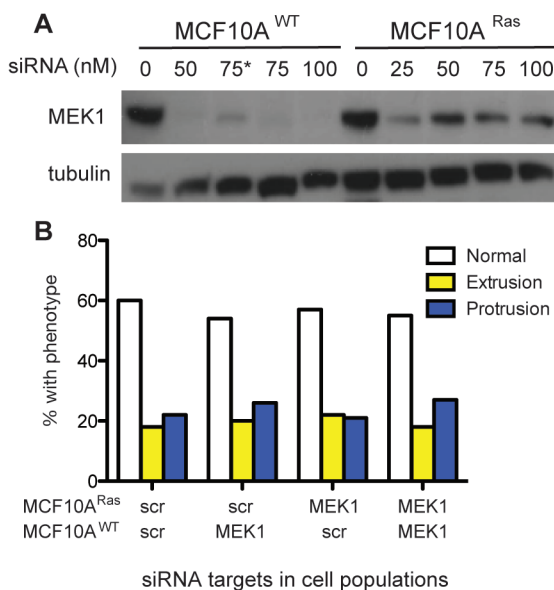


**FIGURE 4-2. RNAi of MEK1 in specific assembly population.** (A) Western blot of MEK1 levels in MCF10A<sup>WT</sup> and MCF10A<sup>Ras</sup> cells treated with siRNA for 72 hours. \* denotes sample treated for 48 hours. scr samples were transfected with 100nM of a scramble control siRNA. (B) Distribution of phenotypes on knockdown with MEK1 or scrambled (scr) siRNA in each assembly subpopulation.

## INVESTIGATING THE ROLE OF PARACRINE SIGNALING MOLECULES

Our observations that protrusions and extrusions occur with heterogeneous assemblies containing either single MCF10<sup>Ras</sup> (MCF10AT) or MCF10A pBabepuro Ras cells suggested that these behaviors arise as a result of differential Ras pathways activation within an epithelial tissue. We hypothesized that altering signals to receptors upstream of Ras could attenuate differences in Ras activity between the two populations. For instance, decreasing upstream signals could dampen the Ras signaling in transformed cells to WT levels. Conversely, increasing upstream signals could bring levels of Ras activation in WT cells closer to that of the Ras-expressing cells. Either of these scenarios can be simulated by manipulating the growth factors that signal through Ras in the culture media.

We first tested whether decreasing growth factor concentrations would alter the frequency of emergent behaviors in heterogeneous microtissues by omitting EGF from the assay medium. Without EGF, assemblies containing single MCF10A<sup>Ras</sup> cells with MCF10A<sup>WT</sup> neighbors decreased the frequency of protrusions but continued to display extrusions (Figure 4-3A). This observation indicated that growth factors can contribute to the frequency of emergent behaviors, possibly by altering the relative levels of Ras activity between the two populations of cells.

To study the effects of global increases in Ras activity, we turned to the MDCK cell system. Unlike MCF10A cells, MDCK cells expressing H-Ras<sup>V12</sup> under pBabepuro LTR were similar to MCF10A<sup>Ras</sup> cells; they do not form invasive structures and maintain their epithelial morphology in 2D and 3D culture (Sakurai et al., 2012). Additionally, 3D cultures of MDCK cells are typically grown in 10% fetal bovine serum (FBS), which contains more Ras-stimulating factors than the 2% horse serum in which MCF10A 3D structures are cultured. Under the standard 10% FBS media conditions, extrusions and protrusions were not observed in any MDCK assembly combinations (data not shown). Cells within the MDCK assemblies also appeared more motile than corresponding MCF10A assemblies, consistent with the notion that media factors were stimulating signaling pathways contributing to motility-based phenotypes in WT MDCK cells (data not shown). When the FBS concentration in MDCK culture was dropped to 3%, however, extrusion and protrusion events were observed (Figure 4-3B). Although the phenotypes were observed to some degree in all assembly types, they were most frequent in the assemblies containing single Ras-expressing cells with WT neighbors. Together, these results suggest that relative differences in Ras activation can be manipulated by changing media components to affect the distribution of emergent behaviors. Future work will aim to develop more controllable and quantitative ways to manipulate Ras activation levels within each of the assembly subpopulations (Figure S4).

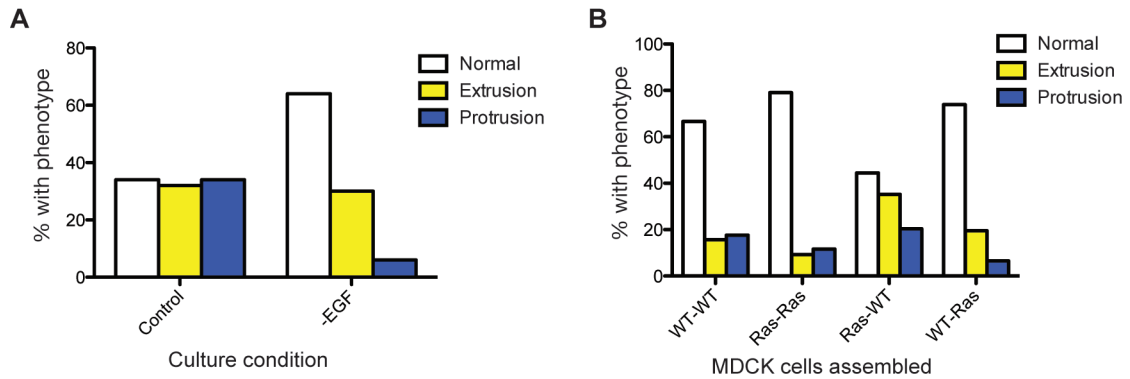


**FIGURE 4-3. Effects of media condition manipulation on phenotype distribution.** (A) Distribution of emergent phenotypes in MCF10A<sup>Ras</sup>/MCF10A<sup>WT</sup> assemblies when EGF is omitted from the media. (B) Distribution of emergent phenotypes in MDCK assemblies in 3% FBS media conditions. No emergent phenotypes were observed in 10% FBS conditions.

As many different signaling pathways can lead to activation of MEK and Akt, paracrine molecules other than EGF may also be involved in the phenotypes. To determine whether other growth factors and cytokines are involved in promoting extrusions and protrusions, we treated heterogeneous assemblies with recombinant TGF $\alpha$ , TGF $\beta$ , and IL-6. These factors were prime candidates for study as they have previously been shown to affect motility of breast epithelial cells (Leslie et al., 2010; Matthay et al., 1993; Seton-Rogers et al., 2004). Similar to the manipulation of EGF and serum concentrations, addition of these factors could either increase or decrease the frequency of emergent behaviors by affecting the relative activity of specific pathways between Ras and WT cells. Treatment of assemblies in complete 3D culture media with TGF $\alpha$  did not lead to dramatic differences in observed phenotype frequencies (Figure 4-4A). Treatment with IL-6 resulted in a modest decrease in both phenotypes, while treatment with TGF $\beta$  led to a modest decrease in extrusions (Figure 4-4A).

Because we had shown that EGF concentration is an important determinant of the distribution of emergent phenotypes, we hypothesized that the effect of EGFR signaling could mask effects of these other molecules in normal culture media. We therefore also treated assemblies with exogenous soluble factors in media lacking EGF (Figure 4-4B). Under these conditions, neither IL-6 nor TGF $\beta$  could rescue the protrusion phenotype. In contrast, addition of TGF $\alpha$  restored the frequency of protrusions to levels comparable to or higher than that observed in EGF-containing conditions. This is perhaps not surprising, as TGF $\alpha$  is also a ligand for EGFR. Together, these data are consistent with the notion that EGFR signaling is necessary for the protrusion phenotype. They also indicate that exogenous IL-6 and TGF $\beta$  signaling are insufficient as single agents to induce the protrusion phenotype, though these and other paracrine signaling molecules may still be involved in regulating the distribution of phenotypes.

To determine whether these cytokines and growth factors are exchanged between cells under the normal culture conditions, we treated heterogeneous assemblies with neutralizing antibodies against EGF, IL-6, TGF $\alpha$ , and TGF $\beta$  with the goal of blocking paracrine signaling through specific pathways between the two cell populations (Figure 4-4C). Unexpectedly, we observed an increased incidence of protrusions on treatment with the control goat IgG antibody compared to previous experiments in the absence of antibodies. Treatment of assemblies with neutralizing antibodies against EGF, IL-6, or TGF $\beta$  all resulted in a slight decrease in protrusions compared to the IgG control and a slight increase



in extrusion frequencies. More replicates of these experiments are required to determine whether these changes are significant.

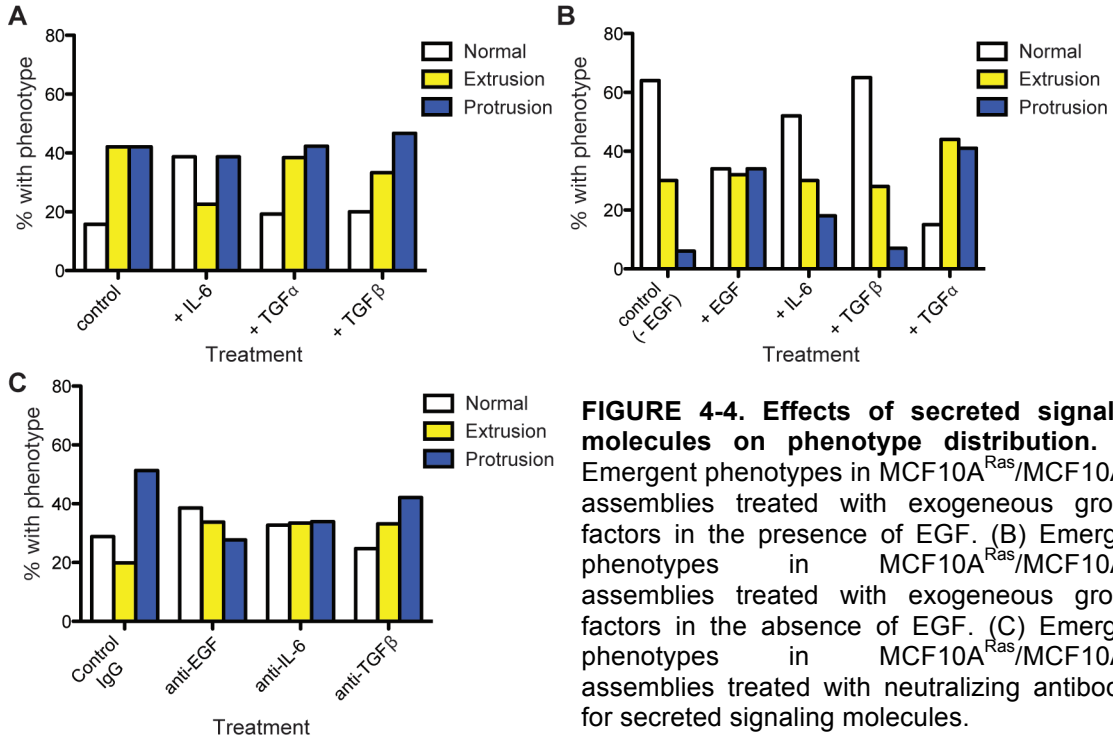


**FIGURE 4-4. Effects of secreted signaling molecules on phenotype distribution.** (A) Emergent phenotypes in MCF10A<sup>Ras</sup>/MCF10A<sup>WT</sup> assemblies treated with exogenous growth factors in the presence of EGF. (B) Emergent phenotypes in MCF10A<sup>Ras</sup>/MCF10A<sup>WT</sup> assemblies treated with exogenous growth factors in the absence of EGF. (C) Emergent phenotypes in MCF10A<sup>Ras</sup>/MCF10A<sup>WT</sup> assemblies treated with neutralizing antibodies for secreted signaling molecules.

## HETEROGENEITY IN E-CADHERIN EXPRESSION IN MCF10A<sup>RAS</sup> CELL LINE

One possibility for the difference between extrusion and protrusion phenotypes is intrinsic heterogeneity of the MCF10A<sup>Ras</sup> line. Recent studies of PI3K activity in MCF10A cells indicate that signaling heterogeneity exist within a cell line population (Yuan et al., 2011). Since the MCF10A<sup>Ras</sup> line was derived by selection of antibiotic-resistant, HRas<sup>V12</sup>-transformed MCF10A cells, MCF10<sup>Ras</sup> cells may also have cell-to-cell variability in other biological processes that biases individual cells towards one behavior in heterogeneous assemblies.

While 2D monolayers of MCF10A<sup>Ras</sup> cells look similar to MCF10A monolayers at confluence, morphologically distinct populations are noticeable within the MCF10A<sup>Ras</sup> line at lower densities (data not shown). Specifically, aside from cells with typical cobblestone, epithelial morphology, we also observed cells that appear more elongated and less adherent, similar to cells undergoing EMT. These cells could be less cohesive due to defective or lower levels of E-cadherin. The lack of cortical  $\beta$ -catenin staining in extruding cells would also be consistent with the existence of a less adherent subpopulation (Figure 3-3D). To test these possibilities, we stained MCF10<sup>Ras</sup> cells expressing H2B-GFP with an anti-E-cadherin antibody. With flow analysis, we noticed that there was indeed a shoulder in the distribution consistent with cells expressing lower levels of E-cadherin that was not detected by Western blot at the population level (Figure 4-5A). Using FACS, we sorted a population of the cells expressing lower levels of E-cadherin (lowest 10%, E-cad<sup>Lo</sup>) as well as a population of cells expressing levels similar to MCF10<sup>WT</sup> cells (highest 30%, E-cad<sup>Hi</sup>). In preliminary studies, we found that heterogeneous assemblies containing E-cad<sup>Lo</sup> MCF10A<sup>Ras</sup> cells displayed much higher levels of extrusion events than assemblies containing cells from the wider MCF10A<sup>Ras</sup> population (Figure 4-5B). To determine whether decreasing E-cadherin levels in MCF10A<sup>Ras</sup> cells would be sufficient to switch cells from protruders to extruders, we attempted to use RNAi to knockdown expression of E-cadherin. Unfortunately, the siRNA pool we used did not decrease levels of E-cadherin (Figure 4-5C), and other approaches such as use

of blocking antibodies or expression of dominant negative E-cadherin may be required to address our question.

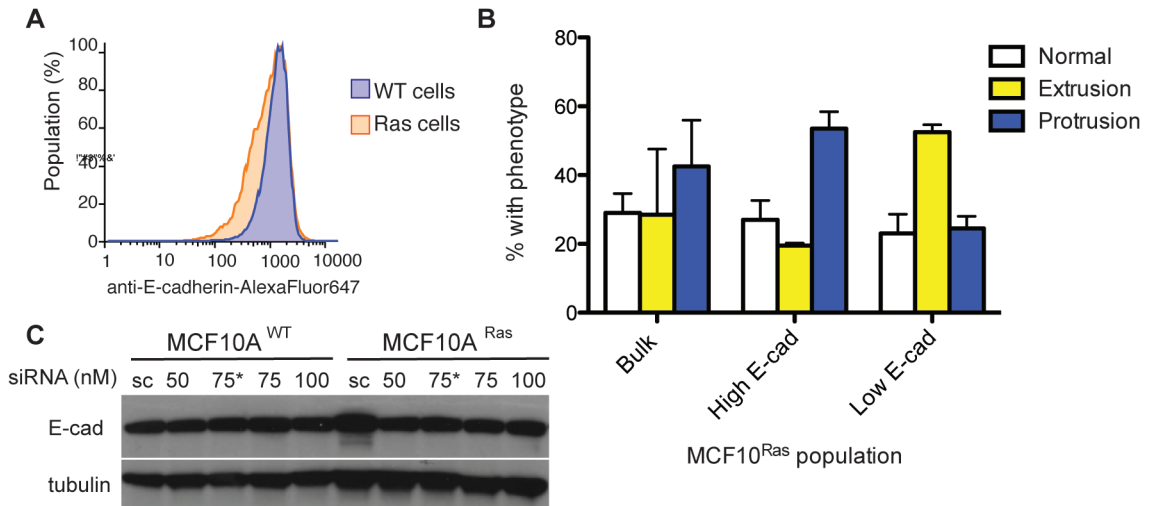


**FIGURE 4-5. Extrusion phenotype associated with low E-cadherin expression of MCF10ARas cells.** (A) Flow analysis of E-cadherin levels in MCF10A<sup>Ras</sup> cells compared to MCF10A<sup>WT</sup> cells reveals a population expressing lower levels of E-cadherin. (B) Phenotype distribution in MCF10A<sup>Ras</sup>/ MCF10A<sup>WT</sup> assemblies made with MCF10A<sup>Ras</sup> cells expressing high or low levels of E-cadherin. Data are expressed as the mean of 2 experiments with error bars representing the S.D. (C) Western blot of E-cadherin levels in MCF10A<sup>Ras</sup> and MCF10A<sup>WT</sup> cells treated with siRNA against E-cadherin at different concentrations for 72 hours.

To further probe the effects of cell-intrinsic factors that could influence the incidence of the emergent phenotypes, we isolated clonal populations from the MCF10A<sup>Ras</sup> line. Consistent with our anti-E-cadherin flow analysis, we observed clones with low and normal levels of E-cadherin by western blot (Figure 4-6A). Our preliminary results indicate that heterogeneous assemblies containing MCF10A<sup>Ras</sup> cells from the clonal populations that express low levels of E-cadherin are also more prone to extrusion events (Figure 4-6B). In contrast,

assemblies containing cells from clonal MCF10A<sup>Ras</sup> populations that express WT-levels of E-cadherin appeared to be more prone to protrusion events. These data corroborate our results with the sub-populations isolated using FACS. While intrinsic differences in levels of Ras, phospho-ERK, and phospho-Akt were also observed across the clones, no correlation between these signals and either of the phenotypes was apparent (Figure 4-6A).

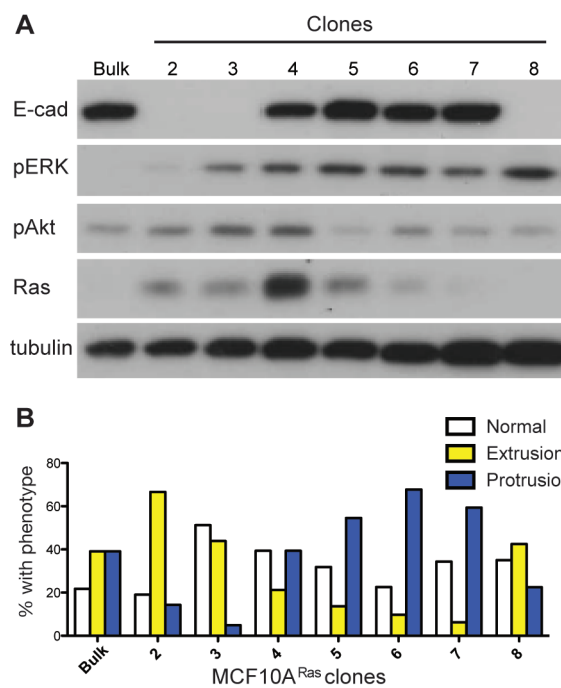


**FIGURE 4-6. Cell intrinsic differences in MCF10A<sup>Ras</sup> clones.** (A) Western blot analysis of E-cadherin and Ras signaling pathways components in a panel of MCF10A<sup>Ras</sup> clones. (B) Phenotype distribution in MCF10A<sup>Ras</sup>/MCF10A<sup>WT</sup> assemblies made with MCF10A<sup>Ras</sup> clones.

## DISCUSSION

Our initial investigation of potential molecular mechanisms involved in the emergent extrusion and protrusion phenotypes has yielded a number of

interesting observations. For one, the phenotypes have differential dependences on effectors downstream of Ras. In MCF10A aggregates undergoing morphogenesis, basal extrusions of single MCF10A<sup>Ras</sup> cells appeared to depend on MAPK but not PI3K pathway signaling. Recently, Hogan *et al.* and Leung *et al.* observed a similar dependence on MEK during apical cell extrusions triggered by activation of Ras or ErbB2, respectively, suggesting that apical and basal extrusions in other systems may be related processes (Hogan *et al.*, 2009; Leung and Brugge, 2012). Motile multicellular protrusions, on the other hand, were dependent on both PI3K and the MAPK signaling pathways similar to multicellular basal protrusions induced by HGF in MDCK cyst tubulogenesis (O'Brien *et al.*, 2004). Because the chemical nature of our approach allows us to systematically incorporate genetically manipulated cell populations, we can use RNAi technology to knock down MEK (1 and/or 2) or PI3K p110 isoforms specifically in either the MCF10A<sup>Ras</sup> or MCF10A<sup>WT</sup> cells to determine which populations require these signaling molecules for the emergent phenotypes. Future work may also use RNAi approaches to study the effects of other Ras pathway signaling molecules such as EGFR or MEK and PI3K effectors on heterogeneous assembly behaviors.

Another key molecular player is the adhesion molecule E-cadherin. The differential preference for extrusions by assemblies made with E-cad<sup>Lo</sup> MCF10A<sup>Ras</sup> cells and protrusions by assemblies made with E-cad<sup>Hi</sup> MCF10A<sup>Ras</sup> cells made it clear that the distribution of phenotypes in assemblies made with the bulk population could at least in part be attributed to subpopulation

differences within the cell line. The correlation with low E-cadherin levels potentially points to a cell sorting phenomena due to differential adhesion as a driving factor for the extrusion phenotype (Steinberg, 2007). The decrease in E-cadherin levels within the MCF10A<sup>Ras</sup> cells may be driven by changes to phosphorylation of E-cadherin interaction partners or through transcriptional regulation via Akt (Grille et al., 2003; Kinch et al., 1995) and may also indicate a type 3 epithelial-to-mesenchymal transition (EMT) that is associated with cancer progression and metastasis (Kalluri and Weinberg, 2009). Though protruding cells retain expression of E-cadherin, their increased motility and sensitivity to growth factor signaling is also reminiscent of EMT or partial EMT (Andrews et al., 2012; Tiwari et al., 2012). It will be interesting to see whether the parallel between previous reports of EMT and the emergent phenotypes we observe will be supported with further molecular studies of the heterogeneous assemblies.

## METHODS

### **CELL CULTURE AND MATERIALS**

MCF10A and MCF10A derivative cells were cultured as previously described in Chapters 2 and 3. MDCK cells were cultured as described in Chapter 3.

### **ANTIBODIES AND OTHER REAGENTS**

Western blot antibodies are listed in Chapter 3. Neutralizing antibodies against TGF $\alpha$ , TGF $\beta$ , EGF, and IL-6 were purchased from R&D Systems and used at 2

ng/mL. Exogenous TGF $\alpha$  at 1 ng/mL, TGF $\beta$  was used at 2 ng/mL, and IL-6 at 5 ng/mL (Peprotech). Sorafenib was a kind gift from Professor Kevan Shokat and used at 10 $\mu$ M. PIK-90 was purchased from Calbiochem and used at 2  $\mu$ M. LY294002 and PD325901 (Calbiochem) were used at 20  $\mu$ M and 200 nM, respectively.

## **CELL LABELING, ASSEMBLY, AND 3D CULTURE**

Cell labeling using NHS-DNA, assembly, and assembly purification protocols are outlined in Chapter 2 with assemblies sorted in culture media containing 1:200 DNase. 3D on-top cultures were performed as described in Chapter 2.

## **MICROSCOPY AND PHENOTYPE QUANTIFICATION**

Live cell imaging and phenotype quantification were performed as described in Chapter 2.

## **FACS OF POPULATIONS EXPRESSING DIFFERENTIAL LEVELS OF E-CADHERIN**

Cells were trypsinized and stained with an anti-E-cadherin antibody conjugated to AlexaFluor647 (BioLegend). Populations expressing high and low levels of E-cadherin were sorted on a FACSAriaII using an 85  $\mu$ m nozzle at 20 PSI.

## **SIRNA KNOCKDOWN**

ON-TARGETplus siRNA pools for MEK1 and E-cadherin were purchased from Thermo and transfected into MCF10A and MCF10A<sup>Ras</sup> cells using Dharmafect

Reagent 1 according to manufacturer's instructions. Media was changed the day following transfection, and cells were lysed 48-72 hours after transfection for Western blotting.



## REFERENCES

Andrews, J.L., Kim, A.C., and Hens, J.R. (2012). The role and function of cadherins in the mammary gland. *Breast cancer research : BCR* 14, 203.

Grille, S.J., Bellacosa, A., Upson, J., Klein-Szanto, A.J., van Roy, F., Lee-Kwon, W., Donowitz, M., Tsihchlis, P.N., and Larue, L. (2003). The protein kinase Akt induces epithelial mesenchymal transition and promotes enhanced motility and invasiveness of squamous cell carcinoma lines. *Cancer research* 63, 2172-2178.

Hogan, C., Dupre-Crochet, S., Norman, M., Kajita, M., Zimmermann, C., Pelling, A.E., Piddini, E., Baena-Lopez, L.A., Vincent, J.P., Itoh, Y., *et al.* (2009). Characterization of the interface between normal and transformed epithelial cells. *Nature cell biology* 11, 460-467.

Kalluri, R., and Weinberg, R.A. (2009). The basics of epithelial-mesenchymal transition. *The Journal of clinical investigation* 119, 1420-1428.

Kinch, M.S., Clark, G.J., Der, C.J., and Burridge, K. (1995). Tyrosine phosphorylation regulates the adhesions of ras-transformed breast epithelia. *The Journal of cell biology* 130, 461-471.

Leslie, K., Gao, S.P., Berishaj, M., Podsypanina, K., Ho, H., Ivashkiv, L., and Bromberg, J. (2010). Differential interleukin-6/Stat3 signaling as a function of cellular context mediates Ras-induced transformation. *Breast cancer research : BCR* 12, R80.

Leung, C.T., and Brugge, J.S. (2012). Outgrowth of single oncogene-expressing cells from suppressive epithelial environments. *Nature* 482, 410-413.

Matthay, M.A., Thiery, J.P., Lafont, F., Stampfer, F., and Boyer, B. (1993). Transient effect of epidermal growth factor on the motility of an immortalized mammary epithelial cell line. *Journal of cell science* 106 ( Pt 3), 869-878.

O'Brien, L.E., Tang, K., Kats, E.S., Schutz-Geschwender, A., Lipschutz, J.H., and Mostov, K.E. (2004). ERK and MMPs sequentially regulate distinct stages of epithelial tubule development. *Developmental cell* 7, 21-32.

Pearson, G.W., and Hunter, T. (2009). PI-3 kinase activity is necessary for ERK1/2-induced disruption of mammary epithelial architecture. *Breast cancer research : BCR* 11, R29.

Sakurai, A., Matsuda, M., and Kiyokawa, E. (2012). Activated Ras protein accelerates cell cycle progression to perturb Madin-Darby canine kidney cystogenesis. *The Journal of biological chemistry* 287, 31703-31711.

Seton-Rogers, S.E., Lu, Y., Hines, L.M., Koundinya, M., LaBaer, J., Muthuswamy, S.K., and Brugge, J.S. (2004). Cooperation of the ErbB2 receptor and transforming growth factor beta in induction of migration and invasion in mammary epithelial cells. *Proceedings of the National Academy of Sciences of the United States of America* 101, 1257-1262.

Steinberg, M.S. (1963). Reconstruction of tissues by dissociated cells. Some morphogenetic tissue movements and the sorting out of embryonic cells may have a common explanation. *Science* 141, 401-408.

Steinberg, M.S. (2007). Differential adhesion in morphogenesis: a modern view. *Current opinion in genetics & development* 17, 281-286.

Tiwari, N., Gheldof, A., Tatari, M., and Christofori, G. (2012). EMT as the ultimate survival mechanism of cancer cells. *Seminars in cancer biology* 22, 194-207.

Voisin, L., Julien, C., Duhamel, S., Gopalbhai, K., Claveau, I., Saba-EI-Leil, M.K., Rodrigue-Gervais, I.G., Gaboury, L., Lamarre, D., Basik, M., *et al.* (2008). Activation of MEK1 or MEK2 isoform is sufficient to fully transform intestinal epithelial cells and induce the formation of metastatic tumors. *BMC cancer* 8, 337.

Wang, S.E., Yu, Y., Criswell, T.L., Debusk, L.M., Lin, P.C., Zent, R., Johnson, D.H., Ren, X., and Arteaga, C.L. (2010). Oncogenic mutations regulate tumor microenvironment through induction of growth factors and angiogenic mediators. *Oncogene* 29, 3335-3348.

Young, A., Lou, D., and McCormick, F. (2013). Oncogenic and wild-type Ras play divergent roles in the regulation of mitogen-activated protein kinase signaling. *Cancer discovery* 3, 112-123.

Yuan, T.L., Wulf, G., Burga, L., and Cantley, L.C. (2011). Cell-to-cell variability in PI3K protein level regulates PI3K-AKT pathway activity in cell populations. *Current biology* : CB 21, 173-183.

## **CONCLUSION AND PERSPECTIVE**

The work described here validates programmed assembly as a powerful approach for building epithelial microtissues with specific types of cell-cell interactions. The utility of the approach was threefold: (i) programmed assembly generated thousands of nearly identical microtissues, thus facilitating quantification of even rare phenotypes associated with cellular interactions among specific subpopulations; (ii) purified aggregates began with pre-defined compositions that can be monitored over time in 3D culture, and (iii) the modularity of programmed assembly allowed for the straightforward modification of microtissue composition to identify which cell populations, and in which proportions, contributed to tissue-level phenotypes. Additionally, aggregate assembly was rapid and resulted in polarized microtissues within 12 hours in 3D culture, thus facilitating identification and characterization of behaviors that emerged shortly after the initiation of cell-cell interactions.

Using the programmed assembly approach, we have begun to probe heterogeneous cell-cell interactions that have been difficult to experimentally model in 3D with current techniques. Notably, we directly investigated the consequences of cell-to-cell variability in Ras activation during the 3D morphogenesis of MCF10A epithelial cells and demonstrated that even modest relative differences in pathway signaling can lead to unexpected emergent behaviors. Remarkably, the microtissues exhibiting the most unusual behaviors, (including basal cell extrusions, motile multicellular protrusions, and hypermotile invasive cell) actually had lower total levels of activated Ras across the cell

population than homogeneous MCF10A<sup>Ras</sup> microtissues that only rarely manifested these phenotypes.

The observation that non-malignant levels of Ras activation can have behavioral consequences in otherwise normal microenvironmental contexts raises a number of interesting issues. First, further investigation into the tissue-level regulation of cell-to-cell variability in Ras activation, particularly in developmental contexts, is warranted. While we have begun to study the mechanisms by which the different cell populations in the heterogeneous assemblies contribute to extrusion and protrusion phenotypes, it remains to be determined how the cell-to-cell variability across the microtissue is detected at the single cell level. Secondly, as cell behaviors are also governed by a number of other signal transduction integrators, we anticipate that low levels of cell-to-cell variability in the activation of proteins other than Ras may similarly result in emergent behaviors within multicellular contexts. Further investigation into the mechanisms by which cell-to-cell variability in Ras and other signaling pathways are maintained or suppressed in different biological contexts will provide greater insight into how tissue heterogeneity impacts multicellular behaviors.

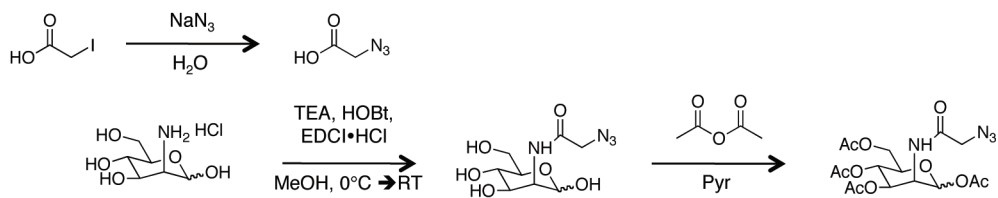
Our findings highlight the need to control for the identity of adjacent cells when studying the effect of genetic, physical or chemical perturbations applied to single mammary epithelial cells. Mammary epithelial cells *in vivo*, however, exist in a complex environment encapsulating many more factors and cell types than we have incorporated into our simplified microtissue model. The development of more complete *in vitro* models for tissues such as the mammary gland will

require a multidisciplinary effort. Fortunately, recapitulating the complexity of human tissues has been the focus of a number of technological advances in fields ranging from microscale tissue engineering to cell biology. Consolidation of such advances, including programmed assembly, may soon allow us to study and manipulate processes such as mammary gland development and breast cancer progression in a comprehensive, *ex vivo* system.

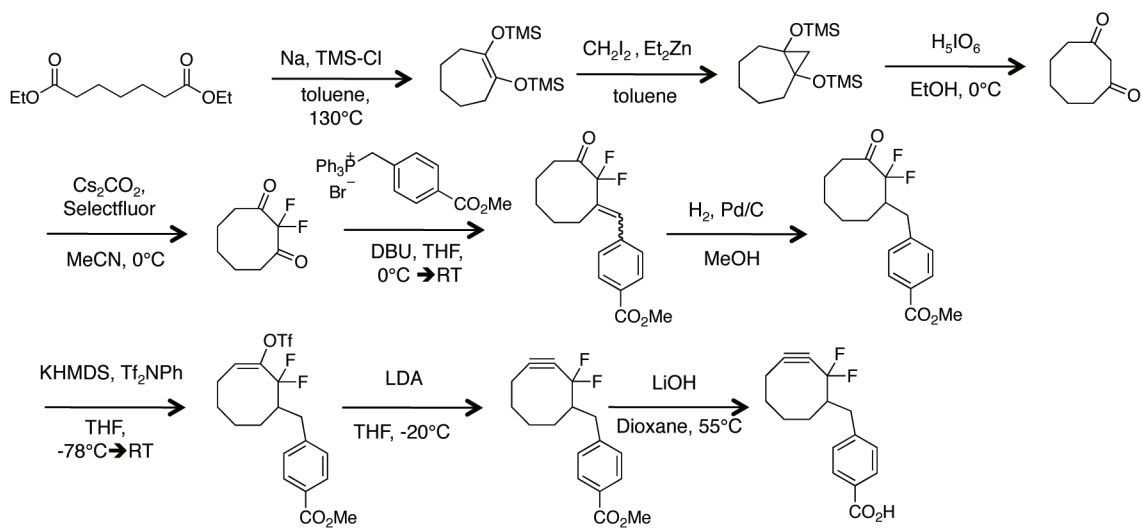


## ***APPENDIX 1***

### ***SYNTHETIC SCHEMES***



**Scheme of synthesis of Per-O-acetylated D-Mannosamine.**

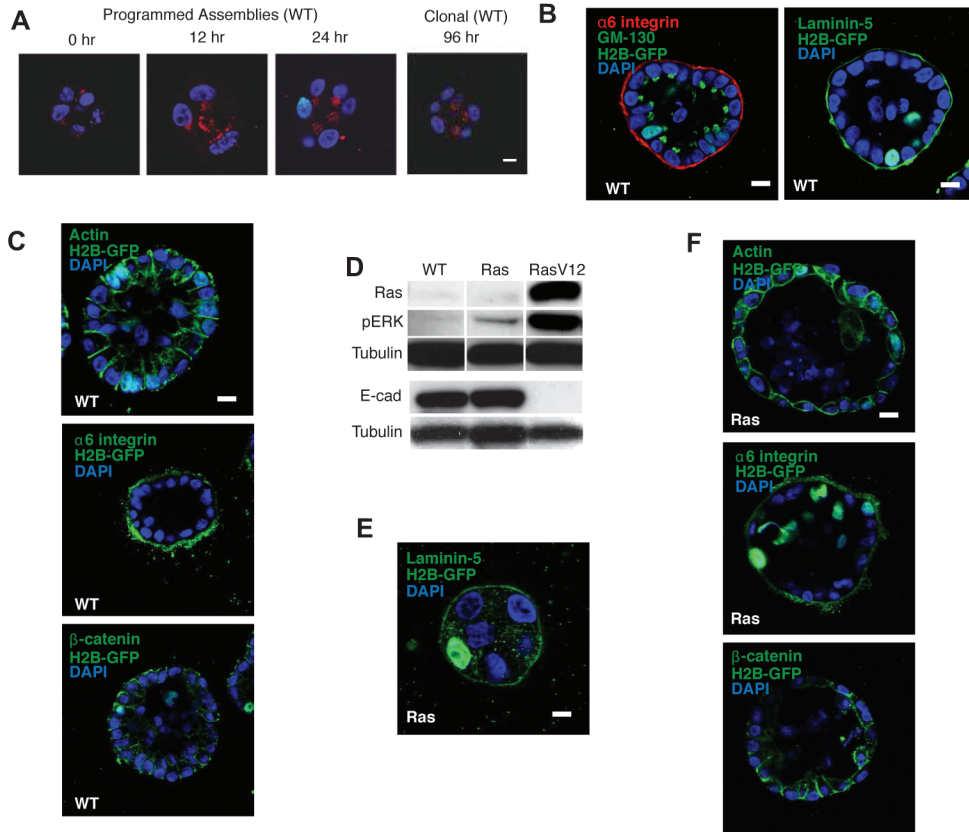


**Scheme of synthesis of second-generation difluorocyclooctyne (DIFO).**

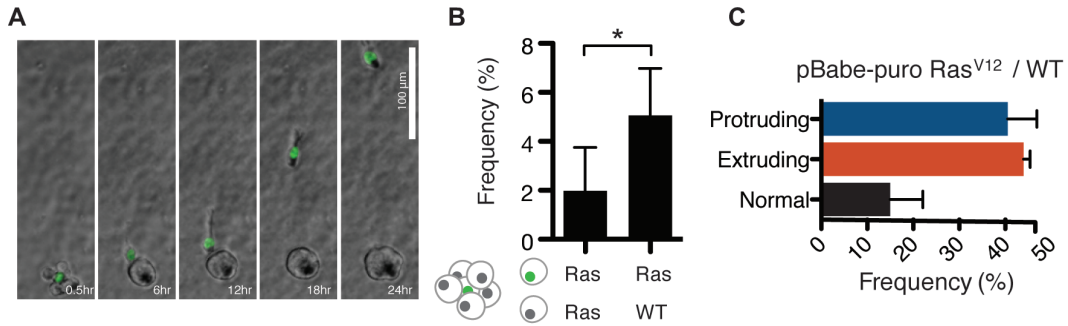
## ***APPENDIX 2***

### ***SUPPLEMENTAL FIGURES AND TEXT***

## SUPPLEMENTAL FIGURES

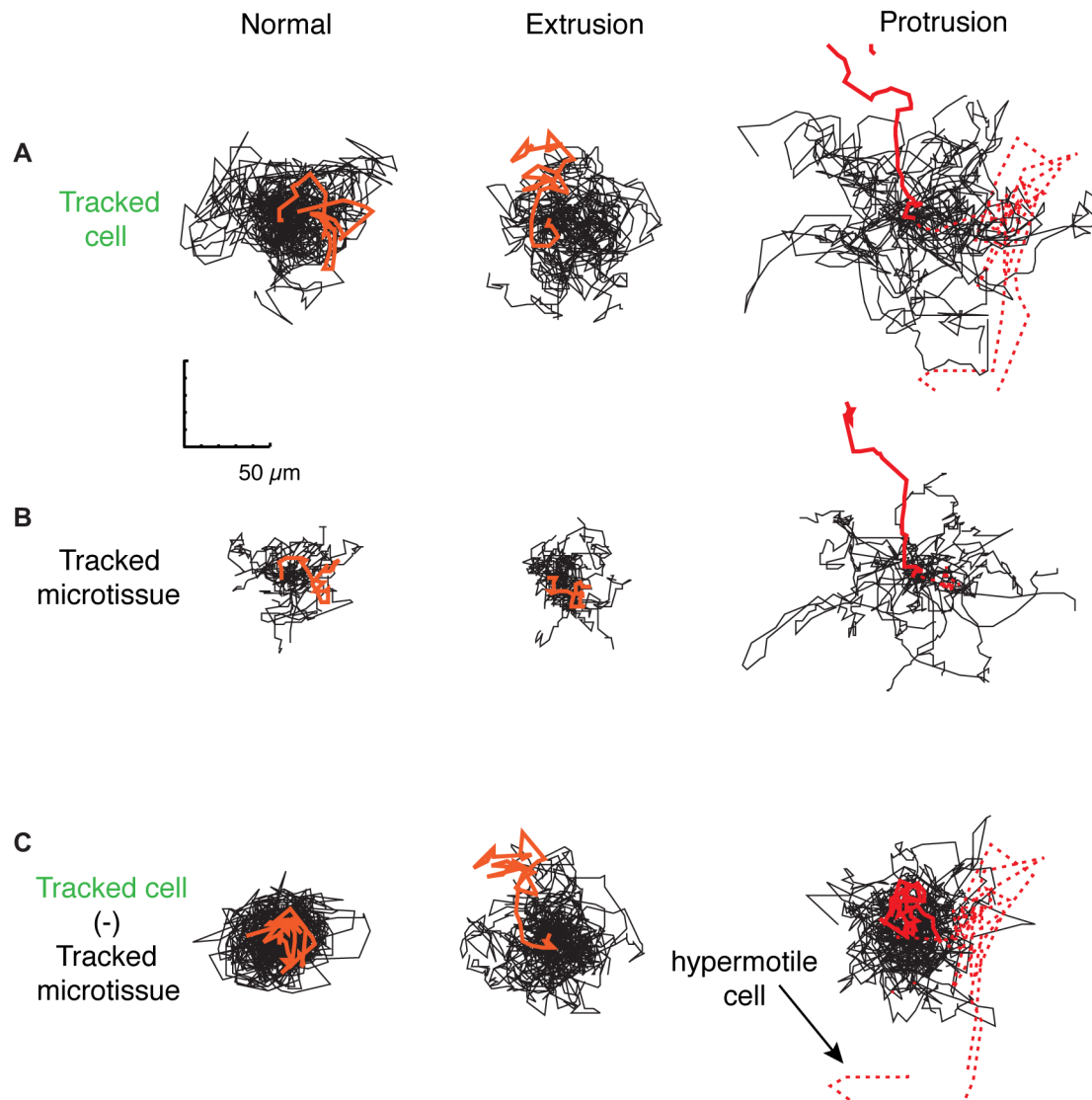


**SUPPLEMENTAL FIGURE 1. Polarity of homogeneous microtissues, Related to Chapter 2.** (A) Representative confocal immunofluorescence images of MCF10A<sup>WT</sup> aggregates stained for GM130 after 0, 12, and 24 hours in 3D culture, and representative immunofluorescence image of similarly sized microtissues grown from single cells for comparison. (B) Representative confocal immunofluorescence images of MCF10A<sup>WT</sup> aggregates stained for polarity markers after 8 days in 3D culture. (C) Representative confocal immunofluorescence images of MCF10A<sup>WT</sup> aggregates stained for polarity markers after 16+ days in 3D culture. (D) Western blots for expression of Ras, phospho-Erk and E-cadherin for MCF10A cells transduced with pBabe-puro H-Ras<sup>V12</sup>. Note that some samples for MCF10A and MCF10A<sup>Ras</sup> are the same as from Figure 3. (E) Representative confocal immunofluorescence images of a MCF10A<sup>Ras</sup> aggregate stained for basement membrane component laminin-5 after 24 hours in 3D culture. (F) Representative confocal immunofluorescence images of MCF10A<sup>Ras</sup> aggregates stained for polarity markers after 16+ days in 3D culture. (scale bar, 10 μm).



**SUPPLEMENTAL FIGURE 2. Characterization of emergent behaviors, Related to Chapter 2.**

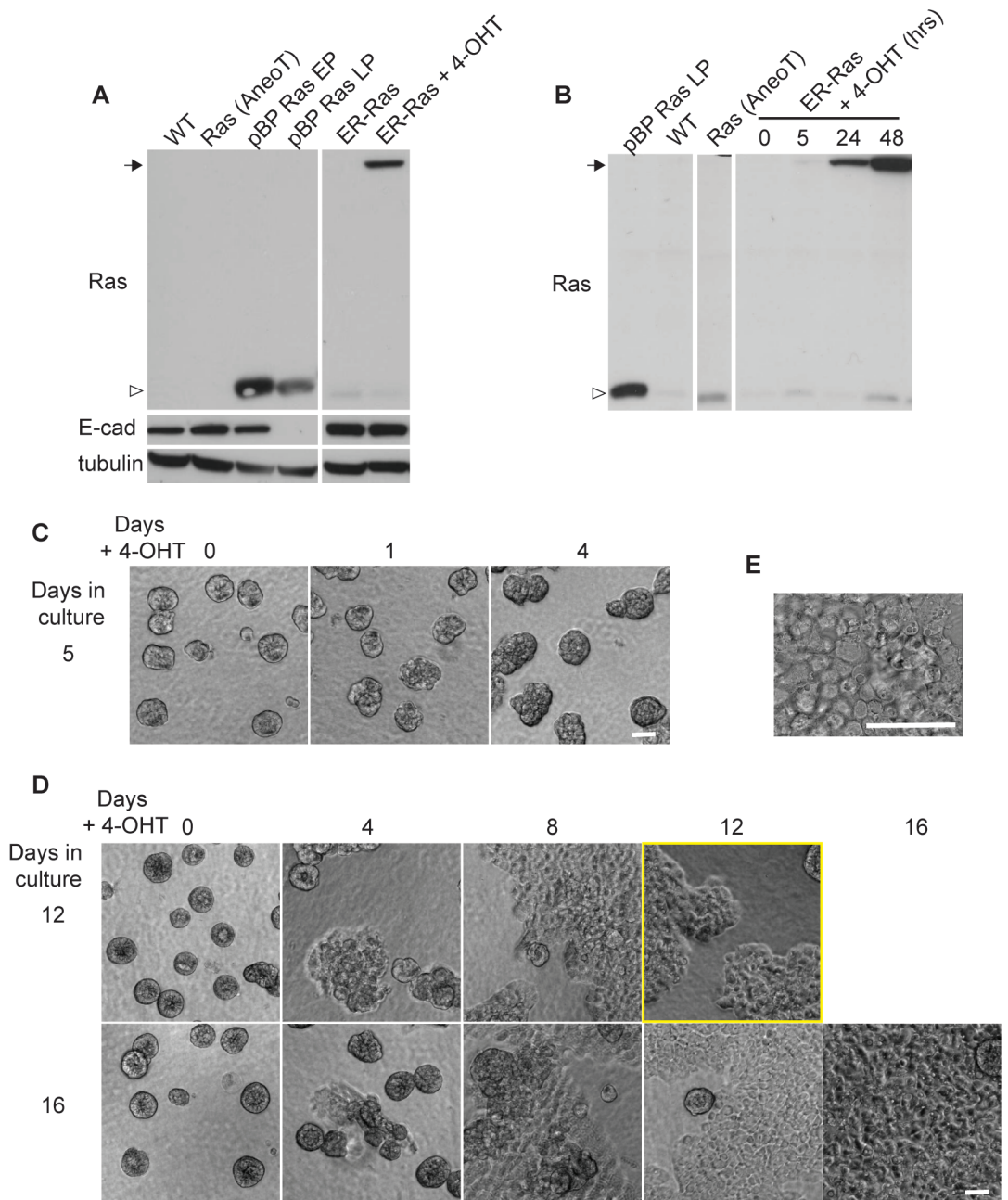
(A) Representative time-series images of a hypermotile MCF10A<sup>Ras</sup> cell from a heterogeneous microtissues. (scale bar, 100  $\mu$ m). (B) Quantification of hypermotile MCF10A<sup>Ras</sup> behavior in microtissues of heterogeneous and homogeneous composition across 532 observations from 4 replicate experiments. Data are shown as the mean with error bars representing the standard deviation of the mean. (C) Quantification of phenotypes in MCF10A pBabe-puro H-Ras<sup>V12</sup>/MCF10A<sup>WT</sup> aggregates. Data are mean values of 3 replicate experiments, with error bars showing standard deviation of the mean.



**SUPPLEMENTAL FIGURE 3. Tracking data for H2B-GFP-expressing MCF10A<sup>Ras</sup> cells in WT microtissues exhibiting normal, basal extruding, or motile multicellular protrusion phenotypes, Related to Chapter 3.** (A) Thirty superimposed cell tracks for the three phenotypes described in Figures 4 and 5. A single representative track is highlighted in red. (B) Thirty superimposed tracks following the centroid of the surrounding WT microtissue. (C) Residual tracks generated by subtracting the WT microtissue track from the track of the corresponding MCF10A<sup>Ras</sup> cell. A track from a cell exhibiting the hypermotile phenotype is indicated by the dashed red line in the protrusion trajectories.

## SUPPLEMENTAL TEXT

One confounding factor in studying extrusions and protrusions in the MCF10A system is the fact that the behaviors are only emergent when MCF10A<sup>Ras</sup> cells express low levels of Ras activation. Towards a more controlled system of Ras activation, we constructed a MCF10A cell line expressing Ras fused to the ligand binding domain of the estrogen receptor (MCF10A<sup>ER-Ras</sup>). In the absence of the 4-hydroxytamoxifen (4-OHT) ligand, the ER-Ras protein is unstable and constantly degraded. Addition of 4-OHT leads to stabilization and accumulation of the protein in a time dependent manner; ER-Ras levels similar to Ras levels observed in MCF10A<sup>Ras</sup> and pBabepuro HRasV12 MCF10A cells can be achieved within 48 hours (Figure S4A and S4B). When grown in 3D in the absence of 4-OHT, MCF10A<sup>ER-Ras</sup> cells form normal structures (Figure S4C and S4D). For modeling how cultured aggregates might respond to acute Ras induction in this system, we treated 4-day clonal cultures with 4-OHT for 24 hours (Figure S4C). Under these conditions, colonies grew slightly larger than untreated controls but remained spheroidal. Addition of 4-OHT for 4 days or more led to spreading of 3D structures into 2D patches that grew progressively larger in area with longer ligand treatment times (Figure S4C, S4D, and S4E). These studies indicate that MCF10A<sup>ER-Ras</sup> cells may morphologically mimic MCF10A<sup>Ras</sup> cells with short induction times, but that they would not be appropriate models for later time point experiments. It remains to be determined whether steady-state, MCF10A<sup>Ras</sup>-like Ras levels can be achieved with an appropriate induction time or with lower ligand concentrations.



**SUPPLEMENTAL FIGURE 4. Characterization of MCF10A<sup>ER-Ras</sup> cells, Related to Chapter 4.** (A) Western blots for Ras (open arrowhead), ER-Ras (arrow), and E-cadherin in MCF10A derivatives. High levels of Ras are observed in pBabepuro H-Ras<sup>V12</sup> MCF10A cells (pBP Ras), though E-cadherin is lost in late passage (LP, more than 2 passages after infection) versus early passage (EP, less than 2 passages after infection) cells. Induction of MCF10A<sup>ER-Ras</sup> cells with 1 $\mu$ M 4-hydroxytamoxifen (4-OHT) for 24 hours leads to accumulation of the ER-Ras protein. (B) Western blots for Ras and ER-Ras in MCF10A derivatives. ER-Ras levels increase in MCF10A<sup>ER-Ras</sup> cells over time on treatment with 4-OHT. (C) 5-day cultures of MCF10A<sup>ER-Ras</sup> cells treated with 4-OHT for the indicated number of days. (D) Later-day cultures of MCF10A<sup>ER-Ras</sup> cells treated with 4-OHT for the indicated number of days. (E) Higher magnification image of 2D growth from 12-day culture highlighted in (D). (Scale bars, 50 $\mu$ m).



## **APPENDIX 3**

### **LIST OF PUBLICATIONS**

**Liu, J.S.;** Gartner, Z.J., 2012. Directing the assembly of spatially organized multicomponent tissues from the bottom up. *Trends in Cell Bio* 22, 683-691. <http://dx.doi.org/10.1016/j.tcb.2012.09.004>.

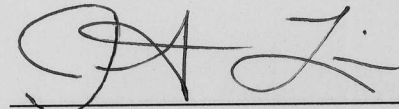
**Liu, J.S.;** Farlow, J.T.; Paulson, A.; LaBarge, M.A.; Gartner, Z.J., 2012. Programmed Cell-to-Cell Variability in Ras Activity Triggers Emergent Behaviors during Mammary Epithelial Morphogenesis. *Cell Reports* 2, 1461-1470. <http://dx.doi.org/10.1016/j.celrep.2012.08.037>.

Selden, N.S.; Todhunter, M.E.; Jee, N.Y.; **Liu, J.S.;** Broaders, K.E.; Gartner, Z.J., 2012. Chemically programmed cell adhesion with membrane-anchored oligonucleotides. *J. Am. Chem. Soc.* 134, 765-768. <http://dx.doi.org/10.1021/ja2080949>.

## Publishing Agreement

It is the policy of the University to encourage the distribution of all theses, dissertations, and manuscripts. Copies of all UCSF theses, dissertations, and manuscripts will be routed to the library via the Graduate Division. The library will make all theses, dissertations, and manuscripts accessible to the public and will preserve these to the best of their abilities, in perpetuity.

I hereby grant permission to the Graduate Division of the University of California, San Francisco to release copies of my thesis, dissertation, or manuscript to the Campus Library to provide access and preservation, in whole or in part, in perpetuity.

A handwritten signature in black ink, appearing to be 'SAZ', written above a horizontal line.

Author Signature

06/13/13

Date